

RAM

● ROBOTICS
AND
MECHATRONICS

POTENTIAL (PASSIVE) FLIGHT STABILIZATION AND CONTROL MECHANISMS FOR FLAPPING ROBOTIC BIRD FLIGHT

P.W. (Patrick) Bos

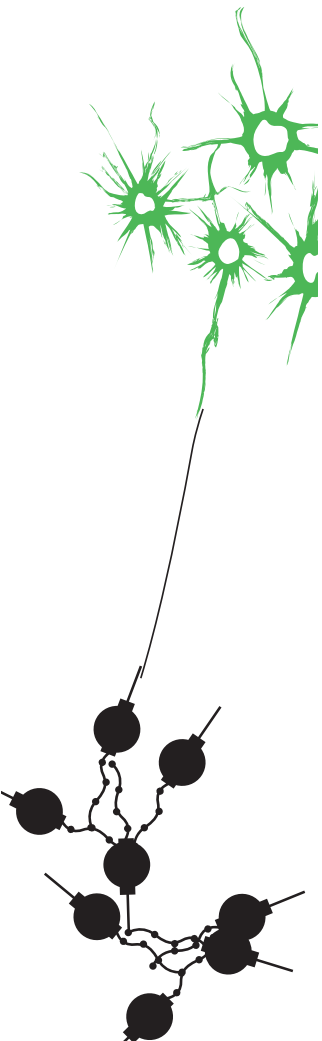
MSC ASSIGNMENT

Committee:

prof. dr. ir. G.J.M. Krijnen
ir. R.S.M. Sneep
ir. L.H. Groot Koerkamp
prof. dr. ir. C.H. Venner
dr. H.S. Bindra

October, 2022

047RaM2022
Robotics and Mechatronics
EEMCS
University of Twente
P.O. Box 217
7500 AE Enschede
The Netherlands



Contents

List of Symbols	3
Acronyms	4
1 Introduction	6
1.1 Background	6
1.2 Problem Analysis	7
1.3 Research Questions	7
1.4 Previous Work	7
2 Theory	10
2.1 The Avian Wing	10
2.2 Perching Manoeuvre	12
2.3 Aerodynamics	13
2.4 Wind Tunnel Testing	16
3 Method and Approach	22
3.1 Static Testing Using a Load Cell on an Airfoil	22
3.2 Dynamic Testing Using the PTV Setup on the RoBird Wing	25
4 Results	30
4.1 Static Testing Using a Load Cell on an Airfoil	30
4.2 Dynamic Testing Using the PTV Setup on the RoBird Wing	35
5 Discussion	40
5.1 Static Testing Using a Load Cell on an Airfoil	40
5.2 Dynamic Testing Using the PTV Setup on the RoBird Wing	41
5.3 Static Testing Using the PTV Setup on a 3D Printed Wing	44
6 Conclusion	45
6.1 Static Testing Using a Load Cell on an Airfoil	45
6.2 Dynamic Testing Using the PTV Setup on the RoBird Wing	45
7 Recommendations	46
8 Appendix	47
8.1 Measurement plan for the static experiments in the small wind tunnel 3.1	47

List of Symbols

ϵ	Total Blockage Factor	
ϵ_{sb}	Solid Blockage Factor	
ϵ_{wb}	Wake Blockage Factor	
Λ	Factor depending on the shape of the profile	
λ_2	The lambda-2 criteria	
ρ	Density of Fluid	kg m^{-3}
σ	Factor depending on the relative size between the airfoil and wind tunnel	
A	Flapping Amplitude	m
c	Chord Length	m
$c_{m\frac{1}{4}}$	Pitching Moment at quarter chord	
cd	Drag Coefficient	
cl	Lift Coefficient	
Cy	Cauchy Number	
f	Flapping Frequency	Hz
h	Height of the wind tunnel	m
K	Bulk Modulus of Elasticity	Pa
l	Characteristic Length	m
Re	Reynolds Number	
St	Strouhal Number	
t	Time	s
u	Flow Velocity	m s^{-1}
U_∞	Free Stream Velocity	m s^{-1}
V	Volume	m^3
v	Velocity of Fluid	m s^{-1}

Acronyms

- BICF** Biologically Inspired Covert Feather. 23, 27, 40, 41, 45
- DOF** Degree Of Freedom. 21, 27
- DSV** Dynamic Stall Vortex. 14
- EWT** Educational Wind Tunnel. 21
- HFSB** Helium Filled Soap Bubbles. 17, 26, 35, 43
- LEV** Leading Edge Vortex. 5, 14, 18, 38, 42, 45
- PIV** Particle Image Velocimetry. 9, 26
- PTU** Programmable Timing Unit. 26
- PTV** Particle Tracking Velocimetry. 5, 16, 18, 22, 25–29, 36, 42–46
- RaM** Robotics and Mechatronics. 27
- UAV** Unmanned Aerial Vehicle. 6

Abstract

Birds are able to control their perching and landings manoeuvres very well, during these manoeuvres the covert feathers lift up. In literature it has been shown this lifting can have an influence on the flight characteristics of the wing. Researching on this topic aims to provide a valuable insight into how these aeroelastic devices function and what kind of influence they have on the aerodynamics of the wing. Most research done is on the static case, this work instead focuses on flapping high angle of attack manoeuvres. This work tries to find out how the lifting of the covert feathers during these manoeuvres influence the airflow over the wing. This is done by using Particle Tracking Velocimetry and analyzing the movement of the Leading Edge Vortex for a wing with imitated covert feather flaps. By looking at how different design parameters for these imitated flaps influence the flight characteristics in the static case, a flap is chosen. Through these methods a flap was found that for the static case had an improvement of 35% at an angle of attack of 18° and higher. Using Particle Tracking Velocimetry it was found that for this flap the detachment of the Leading Edge Vortex is delayed by approximately 100 ms. It is recommended to improve the method by adding a force and torque sensor and testing for more flap designs, and scenarios.

1 Introduction

1.1 Background

The world is changing rapidly and with new technologies and ideas being exploited commercially many of these technologies and ideas are becoming cheaper and cheaper and, thus, way more people and startups can afford new and exciting technologies which in turn drives innovation. One of the fields in which this growth in innovation can be seen is the aerospace industry. Many new startups and ideas are being formed and put into production, ranging from spacecraft all the way to drones. For example, Relativity Space aims to build a fully 3D printed Rocket such that parts can be quickly fabricated [1]. Also, a German startup, Wingcopter, just secured almost 40 million euros for their delivery drones [2].

As just indicated, one of the fields where this innovation is happening is that of drones. When people hear the word drone there is often a very specific view in their head, even though the term is actually quite broadly defined. A better description is given by the more commonly used term in the industry: Unmanned Aerial Vehicle (UAV). As the name suggests this can be anything from a large airplane to a flying robot the size of an insect.

One such a startup is the Drone Bird Company. Founded in 2012 as Clear Flight Solutions their focus is on, for example, bird control and wild life monitoring at locations such as airports and for the oil and gas industry. The product that made them very successful was the RoBird. Instead of using static wings to generate lift and a propeller to generate thrust, the RoBird is a robotic bird that actually mimics bird flight and can both generate lift and thrust by flapping its wings [3].



Figure 1: *The deflection of covert feathers as seen on a kestrel [4].*

Even though this RoBird already manages to fly, the exact mechanics of bird flight and other mechanisms the bird uses, is not yet fully understood. To be able to research this and get a deeper understanding of these mechanisms, PortWings was created and was awarded a European research grant of €2.8M. The project will last 5 years and started in 2018. The ultimate goal of port wings is to understand and model bird flight, confirm this experimentally, and finally improve the RoBird in a number of ways such as better flight dexterity, perching manoeuvres and more [5].

Part of the reason why it is so interesting to understand bird flight is because this is a way of using evolution, which is a very powerful (although with limitations) optimization tool. This is especially useful when it comes to flying since there is a lot of optimization to do when it comes to making something fly. For example any weight that is not necessary you want to get rid of since it will have bad effects on the performance. There are many different areas to optimize things in such as more efficient flight, faster flight, more stable flight and so on.

One of the famous examples an engineering improvement that was inspired by nature is the bullet train. The bullet train needed to go through tunnels but it went so fast that upon entering the tunnel there was a loud bang. The eventual solution was inspired by the head of a kingfisher, as these birds can enter the water almost silently.

One such mechanism which could lead to promising improvements are the covert feathers and their role in bird flight and manoeuvres. These feathers have been observed to deploy in for example perching manoeuvres or when flying in a gusty environment, see Figure 1. Furthermore it is hypothesised that birds take advantage of deploying these feathers by them changing the airflow around the wing. Although this topic has already been researched, as can be read in section 1.4, there is still more to be understood about the exact role of these feathers in various scenarios.

1.2 Problem Analysis

Quite some promising research has already been done on the deployment of these covert feathers. One of the more prominent papers that led to this research was the paper by Anna C. Carruthers titled: "Automatic aeroelastic devices in the wings of a steppe eagle *Aquila Nipalensis*" [6]. In this paper various perching manoeuvres of a steppe eagle are analyzed by filming the bird and its wings with high speed cameras. Although focusing more on the ventral covert feathers it is also observed that the dorsal covert feathers are deployed during most of the perching manoeuvres. In the same paper it is observed that the covert feathers react to a gusty environment during a gust-response manoeuvre. It is hypothesized that the covert feathers might play a role in sensing the airflow over the wing of the bird. More information about this research and other research from Carruthers et al. [6] can be found in section 1.4.

From the research mentioned above it is observed that the feathers seem to deploy more so during flapping manoeuvres at high angles of attack. These manoeuvres could therefore tell us more about the working or influence of these feathers. Most literature however (section 1.4) focuses mainly on deployment during stall or deep stall without the wings flapping. Instead, this research is focused more on this feather deployment during these flapping manoeuvres at high angles of attack and by doing so hoping to understand the mechanism better, and possibly even improving existing ornithopters like the RoBird. Thus, the following research questions were composed.

1.3 Research Questions

RQ 1: "How does the lifting of covert feathers during high angle of attack manoeuvres influence the airflow over the wing?"

In order to be able to answer this questions the design of these feathers needs to be determined more clearly. for this goal a second sub question was composed which is stated as follows:

RQ2: "Which of the selected imitated covert feather designs lead to the (largest) improvements in lift at high angles of attack in static flight"

The selected imitated covert feathers are chosen for various reasons which will be discussed in section 3.1.

1.4 Previous Work

Understanding and learning from what has already been done on this topic is very important. The biggest difference between the literature that will be discussed and this research is that this research focuses on the dynamic or flapping regime of bird flight instead of the static regime. Luckily quite a lot of literature on aeroelastic devices or high lift devices such as covert feathers already exists. This section aims to give an overview of this research and discuss what exactly has been done and learned.

1.4.1 Automatic aeroelastic devices in the wings of a steppe eagle *Aquila Nipalensis*

Anna C. Carruthers has done a lot of research when it comes to bird flight and the working of specific feathers or body parts. In one such research, a captive steppe eagle was filmed at high speed while executing perching manoeuvres. This way a detailed look could be taken into what happens during this manoeuvre. In this paper it is ultimately concluded that the aeroelastic devices researched, under which also the covert feathers, enhance certain unsteady manoeuvres, such as perching, and could also provide sensory feedback [6].

The main method used as explained were slow motion cameras, and a total of 37 videos were taken from perching manoeuvres [6]. It is important to note that this research is mostly focused on the ventral covert feathers instead of the dorsal covert feathers. Whereas this research and report solely focuses on the dorsal covert feathers. More is explained about these feathers in section 2.1.3. Besides this, these videos and observations were the inspiration for this research and the idea was that understanding this mechanism better could mean improvements for the RoBird.

1.4.2 Covert-inspired flaps for lift enhancement and stall mitigation

In a paper by Duan et al. [7] a design optimization technique was used to find an optimization for a covert-inspired flap attached to the dorsal side of the wing. It was chosen to optimize for lift and the only parameter that was changed was the angle of the flap. Furthermore a discrete vortex model was used to model the lift of this airfoil. Results showed that the flap design could increase lift up to 23% when compared to the same airfoil without the flap. The optimal flap angle that was found was around 12 degrees. It is important to note that the fact that the flap angle was changed means that a rigid / stiff flap is used which can not move with the airflow. This case can be quite different from the case of a flap that is free to move with the airflow [7].

Duan et al. [8] also performed experiments in a wind tunnel with 2 types of covert-inspired flaps. Also more variables were changed in this research, namely: the flap location, the flap type, the airfoil shape, and the angle of the flap for the static case. The results showed again an increase in lift of about 23%. Furthermore it is found that the system is sensitive to the flap location and it is interesting to note that the lift enhancements are attributed to a pressure step on the suction side as described by Bramsefeld et al. [9] [8].

1.4.3 Experimental analysis of passive bio-inspired covert feathers for stall and post-stall performance enhancement

More extensive experimental research was done by Izquierdo et al. [10] In this research self actuating paper flaps were fabricated and put on a static airfoil to see which design and location would increase the lift or delay the stall the most. It was found that a ragged flap design attached at the quarter chord of the airfoil showed the biggest improvements.

Furthermore a ramp-up and hold experiment was done to investigate the quarter chord location flap further and see how it behaves. This was only tested to an angle of attack of 18 degrees max which is "the most representative angle near the stall onset regarding static tests" Also no data has been gathered for the flaps at various locations for the dynamic case. The ramp up speed was altered from 0.18 degrees per second all the way to 9 degrees per second. The results showed that the flaps had a positive effect on smoothing the lift overshoot during ramp up motion. [10].

A good overview and description of the exact method used was given, which made this paper a perfect starting point for the first part of the experiments that were executed. More about this can be read in section 3.1.

1.4.4 Post-Stall Performance Improvement through Bio-inspired Passive Covert Feathers

Altman et al. [11] experimented also with flap length and chord-wise location, furthermore x-foil was used for complementary data. The results showed that there was no universal perfect flap but that it matters per airfoil and/or wing design. An optimum was found for each wing tested and improvements were measured to be between 5% to 30% lift enhancement.

This paper furthermore goes in depth on dividing the flap into multiple flaps, like feathers. The conclusion was that in some scenarios, depending on the airfoil and or flap length and location, it was either beneficial or did not really change anything [11].

1.4.5 Free Flight Observations and Aerodynamic Analysis for Bio-Inspired Optimization

A paper that has somewhat combined the research mentioned before is a paper by Griffin et al. [12]. In this paper a look is taken at the aerodynamics of a cadaver bird wing in a wind tunnel using both force measurements and planar Particle Image Velocimetry (PIV), a measurement technique with which an airflow can be measured quantitatively, see section 2.4.1. Next to that a captive American Kestrel is used for filming the perching and landing manoeuvres to obtain data and gain insight. The results showed that slight variations in wing geometry may lead to larger differences in wing aerodynamics. Furthermore flight and velocity profiles were gathered from the perching and landing manoeuvre of the American Kestrel falcon. [12].

2 Theory

The following section will discuss the theory necessary for understanding the topic surrounding the research done and methods used. This includes theory about the avian wing, the relevant aerodynamics, and theory around wind tunnel testing. An overview of the context of the research and experiments has been given in section 1.

2.1 The Avian Wing

Even though this research is mainly focused on the covert feathers of birds, it is important to first get a proper overview of the wings of a bird. This is because the wings are a very complex part of the bird and contribute to the ability to fly in many different ways. When this context is understood properly, there is also a better understanding of the experiments themselves, which can result in a deeper insight of the results. In this section background information on the anatomy of the wing, the primary flight feathers, and of course the covert feathers, is given.

No two bird species are the same and all have either slightly or very different types of wings. Various reasons have been proposed, ecological reasons such as migratory behaviour, foraging behaviours, sexual selection [13]. But also of course reasons such as size, weight, aerodynamics, and flight behaviour. The fact that there are so many different types of bird and bird wings makes analysing them a very complex problem. Partially for this reason a simplification is made by looking at only one type of bird / bird wing. As was described in section 1 the RoBird is based on the Peregrine Falcon and therefore the baseline, this however does not mean of course that the research is limited to only this bird.

2.1.1 Anatomy

Visually, the biggest parts of the bird wing are its primary and secondary flight feathers. These are the longest and largest feathers on the wing and these will be discussed in more detail in section 2.1.2. The wings are primarily build up around these feathers. The bones or skeleton of the bird forms the main rigid structure, attached to these are its muscles and main flight feathers. The skeletal structure of the wings of a bird is very similar to the arms of a human and this comparison is often made in literature to make things more intuitive. This is indicated in Figure 3. A more in depth look into the anatomy of the wing of a rock pigeon and more specifically the way the feathers are attached to the birds muscles and or bones, is taken in the study by Tobin L. Hieronymus [14].

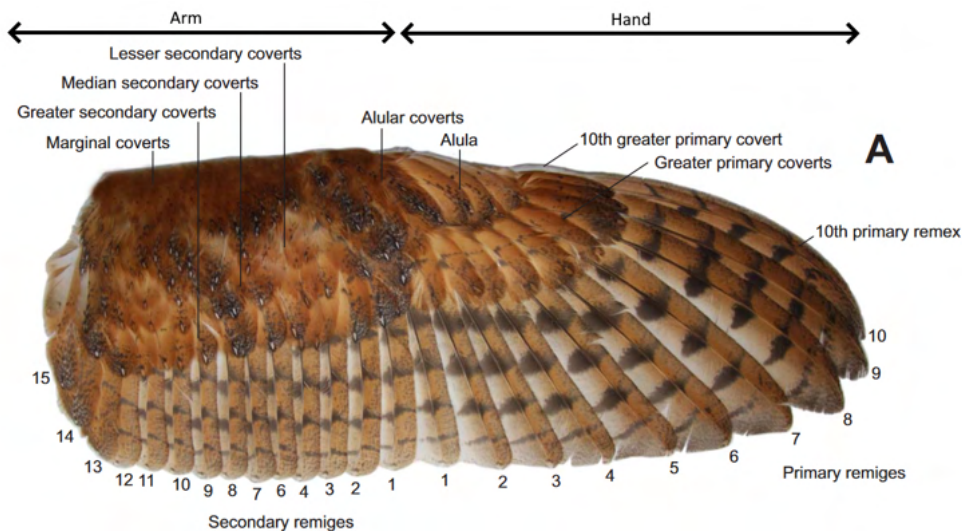


Figure 2: *The wing of a barn owl with the corresponding terms and feather numbering [15].*

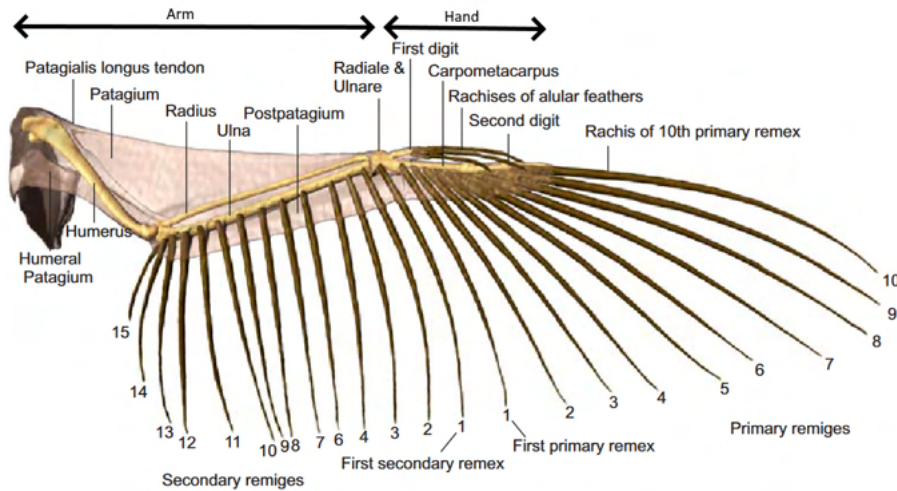


Figure 3: *The underlying bone structure of the same barn owl wing, again with the corresponding terms [15].*

2.1.2 Wing Feathers

To see how the layout of the covert feathers is categorized some more context is needed about the wing and the other feathers, which this section aims to provide. The main way that feathers are distinguished is by their function, this groups them in the following way, as shown in Figure 2. The first group are the flight feathers also called remiges. These consist of the primary flight feathers, also called the primaries and the secondary flight feathers called the secondaries. The primaries and the secondaries are mostly distinguished by where they are attached to the birds wing. As is shown in both Figures 2 and 3 the wing of a bird consists of an "arm" and "hand" section, furthermore the feathers are counted starting from the "wrist" of the wing. Thus resulting in the numbering also shown in the figure.

The remiges are attached to each other and the rest of the wing through multiple smaller ligaments and muscles. The way the feathers are attached makes it such that the bird has control over the remiges, and is able to use this to its advantage during flapping flight [14]. Similar muscle structures are found for the covert feathers which could mean the coverts are also actively controlled.

Other feathers that are less important but still interesting to discuss are the filoplumes and the tertiary feathers. Filoplumes are tiny hairlike feathers that sit at the base of other larger feathers such as the coverts and the remiges. It is proposed in literature that these feathers might have a sensing function for the bird to sense the airflow conditions over the wing. And there are quite some papers such as the one from Necker et al. [16] that show there can be sensory feedback from this feather. This has also been hypothesized to be a function of the covert feathers.

Tertials are the remiges closest to the body of the bird as can be seen in Figure 4. They are differently defined than the secondaries because instead of being attached to the ulna they are attached to the humerus. However their exact definition is not as straight forward as it seems partially, since the term tertials, tertiary feathers and tertiaries are all differently used in literature as can be read about in more detail in an article by Scott Hickman [17].

2.1.3 Covert Feathers

Covert feathers are the feathers that, as the name suggests, cover the wing where the flight feathers attach to the bones and muscles. The main function of these feathers is to streamline or smoothen the shape of the wing, since the aerodynamics are very sensitive to the shape and structure of

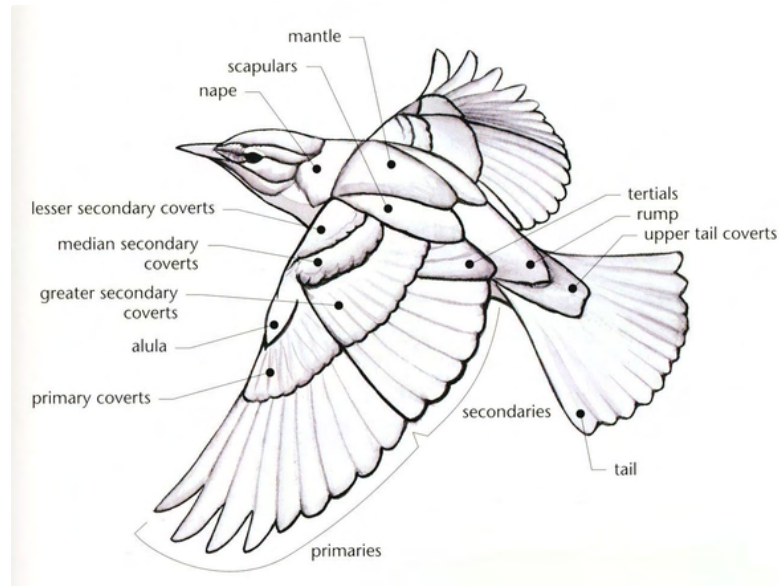


Figure 4: *The layout of the covert feathers [19].*

a surface [18]. Covert feathers are both on the dorsal side as well as on the ventral side. The paper by Carruthers et al. [6] that was discussed earlier in section 1.4.1 focused on these ventral covert feathers, instead this work looks at the dorsal side. On the dorsal side, the feathers are further categorized into 4 different regions of covert feathers as can be seen in Figure 4. Named by their location relative to the remiges the covert feathers above the primaries are called the primary coverts. Similarly the coverts above the secondaries are called the greater median and lesser secondary covert feathers.

The deployment of the covert feathers during a landing or perching manoeuvre has been observed a multitude of times. Carruthers et al. [6] filmed the steppe eagle and observed the deployment of mostly the greater and median secondary coverts. Christopher filmed an American kestrel and observed of the secondary coverts first the lesser coverts lifted, then the median and lastly the greater coverts, all throughout the perching manoeuvre [20]. Lastly in Duan et al. [7] a clear example of the deployment of coverts for the case of an owl is shown. This work focuses primarily on the primary and greater secondary coverts since these show the largest deflection during these manoeuvres

2.2 Perching Manoeuvre

Birds need to rest, they do so on various locations, depending on the bird and the surroundings. Unlike planes, birds can land on a single spot, meaning they do not need much space to stop on the ground or tree itself but instead are almost immediately stationary when touching down. Birds are able to do this by performing the so called perching or landing manoeuvre. This manoeuvre is not exactly defined and can look slightly different depending on the scenario, its surroundings, and the species. For example, the bird can land on the ground and therefore not be able to dive lower than the perch location, the bird can glide towards the perch or flap its wings at the end of the manoeuvre. The trajectory used for this work is the one shown in blue in Figure 5. More can be learned by looking at examples of bird that do this manoeuvre. KleinHeerenbrink et al. [21] recorded over 1500 landings of birds in a controlled environment. It was found that the "swooping" motion also called "undershoot" is used mainly by larger birds to minimize the time spent after stalling, and thus minimizing the distance over which high lift coefficients are required. Also it was mentioned that during the upwards pitching part of the trajectory no real flapping was done by the

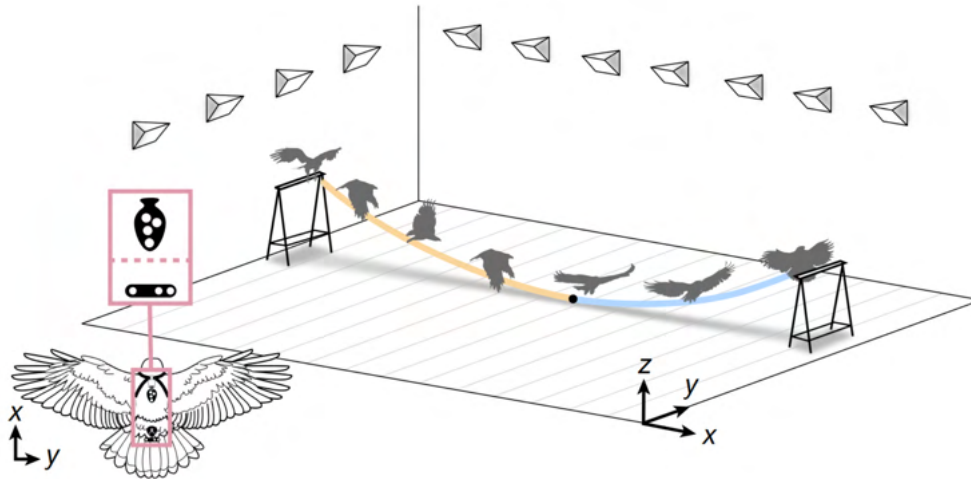


Figure 5: A schematic overview of the trajectory of a perching manoeuvre [21].

bird but instead minor corrective control inputs were given and there were no wing beats supplying thrust to offset drag.

Carruthers et al. [6] recorded a total of 37 landings of which a little more than half were done in an outside environment, and the rest inside. An interesting finding in this research is that the bird seems to prefer to flap its wings during indoor perching manoeuvres, as it always had the flapping type of approach on the inside landings. Outside the bird used mostly the gliding type of approach, and would occasionally flap [6]. This is a rather stark contrast to the findings of KleinHeerenbrink et al. [21] Since in this paper all the landings were also done inside but as mentioned before, no flapping was observed except for minor adjustments. On a side note, all of these landings were inside so no conclusion can be made on what this specific bird would have done in the outside case.

Both papers by Carruthers et al. [6], and Griffin et al. [20] observed the deployment of the dorsal covert feathers during these perching / landing manoeuvres. This is the phenomenon that will be the focus of this research and the experiments done. During these manoeuvres birds gradually change from a flying state to a non flying state during which they undergo dynamic stall which will be explained in the next section.

2.3 Aerodynamics

2.3.1 Dynamic Stall

During a perching manoeuvre birds can have angles of attack close to 90% [6]. In a static scenario this would of course be a deep stall scenario, as for example some airfoils with lift devices deployed such as flaps can only manage around 25° maximum before they transition to stall. When instead of the static case a rapid pitch up motion is performed the stall that happens is very different, this scenario is called dynamic stall. Carr et al. [22] managed to do a detailed analysis of this dynamic stall process using a NACA0012 airfoil, which is one of the more standard symmetric airfoils. As also noted by this paper: "The vortex shedding process is most obvious characteristic of dynamic stall" and this is an important observation as this is one of the core principles used in the experiments. The analysis that was done will be discussed briefly based on Figure 6 and the full analysis can be found in the research by Carr et al. [22].

- a) Static stall angle is exceeded, with the lift coefficient (c_l) for the normal case shown as the dotted line.
- b) Flow Reversal starts at the back of the airfoil
- c) There are indications of eddies moving down the airfoil since the smoke pattern is wavy
- d) The flow reversal continues moving forward towards the leading edge
- e) A vortex starts to form near the leading edge of the airfoil, this is also the beginning of the dynamic stall
- f) c_l rapidly increases and exceeds $2\pi\alpha$ which is normally the static limit for c_l
- g) The vortex grows and "rolls off" the airfoil, this is called moment stall
- h) c_l keeps increasing to the maximum value after which the value drops very quickly
- i) maximum negative coefficient of moment as the vortex passes of the trailing edge
- j) full stall is reached

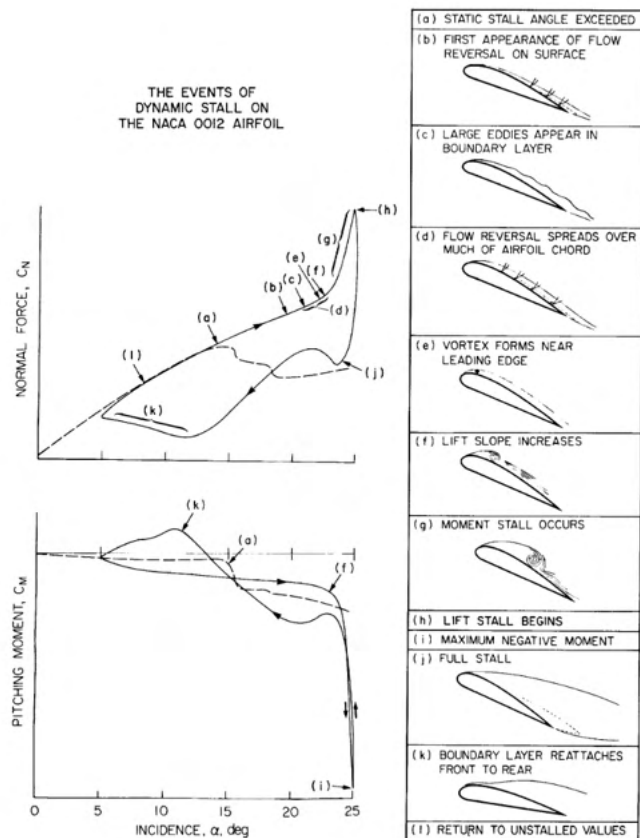


Figure 6: A schematic overview of dynamic stall [22].

From this process of dynamic stall there are two main take-aways in context to the research. Namely the flow reversal more at the beginning of the process and later the vortex structure that forms and moves from the leading edge towards the trailing edge and grows. Since this vortex plays a rather important role it is discussed in more detail in 2.3.2.

2.3.2 Leading Edge Vortex

The Leading Edge Vortex (LEV) or in the context of dynamic stall also called the Dynamic Stall Vortex (DSV); aerodynamically this vortex is one of the most interesting parts about dynamic stall. It is during the existence of this vortex that the lift slope in Figure 6 increases very quickly (images f to g). This vortex is considered to be generated by the flow reversal rapidly moving towards the leading edge while the free stream flow is still going from the leading edge towards the trailing edge. This shearing action can be considered the primary reason for the formation of the DSV [22]. One of the reasons why the lift slope is increased when this vortex exists is because of the increase in suction pressure due to the clockwise rotation (as shown in Figure 6 G) of the DSV [23]. Furthermore, an interesting relation that was found, was that a larger angle of attack at the end of the dynamic stall cycle would shield the vortex more from the free stream making it attached to the airfoil for a longer time. Two more reasons are suggested for the increase in lift during the existence and movement of the DSV. First it is suggested that the DSV effectively changes the

camber of the airfoil because of which the characteristics of the "new airfoil" are different and produce more lift at higher angles of attack. Secondly the Magnus effect is thought to maybe be the reason behind or to contribute to the generation of more lift [23].

2.3.3 High lift devices

Generally speaking high lift devices are used to change the characteristics of the airfoil by moving certain parts or structures around the airfoil. This could for example create a different effective airfoil shape with different characteristics or could change the airflow by, for example a duct or vortex generators. All of these have influence on the aerodynamic characteristics of the airfoil and could be beneficial for e.g. landing and or taking off.

In the case of the covert feather, it is a structure that deploys as a function of the flow reversal that happens during stall or dynamic stall. This means it is able to deploy passively and it has been observed to also be able to influence the airflow around the wing. The properties of these covert feathers have an influence on how this airflow is exactly influenced [24].

2.3.4 Dimensionless Numbers

In aerodynamics there are many variables that have an influence on the situation such as temperature, pressure, flow velocity etc. These variables together say something about the conditions of the environment, which can be expressed in several dimensionless numbers. Using these numbers it can be made sure that the test case will be representative.

Reynolds Number

The Reynolds number is arguably the most popular dimensionless number in aerodynamics, since it is almost always of importance, especially when testing at scale in a wind tunnel. The number is a measure for the ratio between the inertial and viscous forces of the flow [25]. The Reynolds number is defined as follows:

$$Re = \frac{\rho v l}{\mu} \quad (1)$$

Where ρ is the density of the fluid, v is the free stream velocity of the fluid, l is the characteristic length, in this case the chord, and finally μ is the dynamic viscosity of the fluid. Some typical Reynolds numbers are for large aircraft between 10^7 and 10^9 , for light aircraft between 10^6 and 10^7 , for large birds between 10^5 and 10^6 , and insects can go all the way down to 10^3 [26]. All of these examples can generally operate at wider range of Reynolds numbers of course, however this gives some indication of typical values.

Strouhal Number

The Strouhal number is another dimensionless number that gives a relation between the flapping and the free stream velocity, or the air speed of for example a bird. The Strouhal number is defined as follows:

$$St = \frac{fA}{U_\infty} \quad (2)$$

Where f = the flapping frequency, A = the flapping amplitude, and U_∞ = the free stream velocity or in this case wind tunnel speed. It was found that many birds and insects in cruise flight range between a Strouhal number of about 0.2 and 0.4 [27]. For landing or perching manoeuvres there is no real data on what kinds of Strouhal numbers are achieved. However, the velocity will be lower during landing, which would increase the Strouhal number. The flapping frequency and amplitude both will become more irregular but also most likely larger based on the footage in literature (section 1.4). This makes the Strouhal number most probably larger than that in the case of flapping flight.

Cauchy Number

The Cauchy Number can be used for insight in the interaction between a solid and a fluid. It is defined as the ratio between the inertial forces and compressibility. The Cauchy number is defined as follows:

$$Cy = \frac{\rho u^2}{K} \quad (3)$$

Where ρ is the density of the fluid in kg m^{-3} , u is the flow velocity in m s^{-1} , and K is the bulk modulus of elasticity in Pa [28].

Unlike the first of these two variables the bulk modulus of elasticity does not speak for itself in this context. Out of this specific context it is defined as follows:

$$K = -\frac{\delta p}{\delta V/V} \quad (4)$$

Where δp is a small increase in pressure and δV is a small increase in the original volume V [28]. As can be seen in this equation the bulk modulus of elasticity is a ratio between a change in pressure and a change in volume of the specific material. Which can be described as the degree of compressibility of a material.

What is used instead in some cases is the Youngs modulus, which is just like the bulk modulus of elasticity one of the elastic moduli. This however can be a more interesting number for analysing the interaction between a solid and a fluid. In the case of the thin flaps it can be combined with a slenderness ratio.

2.4 Wind Tunnel Testing

In an ideal world all experiments would be done in the exact situation you are testing them for. However doing experiments on the wing of an airplane or a bird is generally not possible. Wind tunnels are the closest attempt we have at creating a suitable test environment which can recreate many scenarios. Of course as with any test setup, since it is not the ideal case the data you get might need to be compensated for certain effects or understood carefully in order to make the right conclusions.

The wind tunnels used in this research are described in more detail in section 3. The flow velocities used are low and both wind tunnels are not capable of high enough velocities to create compressible flow. The rule of thumb is generally that velocities below $M < 0.3$ are incompressible [25]. For this reason for all the experiments that were executed it can be assumed that the flow is incompressible.

2.4.1 Particle Tracking Velocimetry

Particle Tracking Velocimetry (PTV) is a measurement technique that can be used to measure an airflow quantitatively. This has a number of benefits over a technique such as using smoke or a force balance to see the airflow or measure its effect. With PTV it is possible to follow and measure individual particles in the airflow to see how the airflow moves. The setup consists of four parts: the illumination system, the capture system, the bubble generator system, and the software. How all of these parts work and together function as one measurement system will be explained in this section, the actual devices used will be discussed in section 3.2.

The Capture System

The capture system consists of four high speed cameras. Normal cameras would not be able to have a high enough shutter speed for the bubbles to be visible, instead they would then become vague streaks like a blurry picture. Furthermore because the particles move such a small amount between the frames it is possible to track them in space and time. Due to the high frame rate the bubbles move only a small amount between every frame. Because of this, and the fact that the

bubbles can be seen by at least three cameras at the same time, the location of the bubble and its path can be determined by the software. To be able to track the particles in 3D space only three cameras are needed, however the fourth camera improves the accuracy and measurement range significantly, and this is also the reason why almost all setups use four cameras. Furthermore it makes sure that when particles are blocked for one of the cameras still three other cameras can detect the particle and can thus be tracked.

The entire measurement range where the bubbles need to be tracked needs of course to be in focus. Furthermore the optics that are used make the image such that the measurement zone is in focus. This is done using various optics and what is called a scheinpflug. The working of a scheinpflug can be seen in Figure 7, it makes sure that the image plane, even though taken from the wrong angle, is in line with the sensor plane such that the entire image is in focus. These of course need to be calibrated. The lenses themselves fitted to the scheinpflugs make sure the depth of field is correct and as large as the desired measuring range.

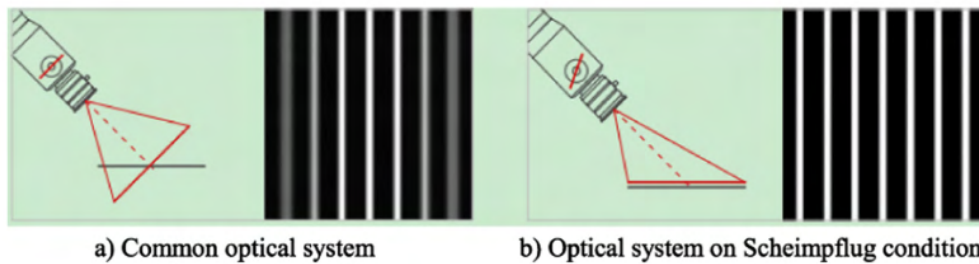


Figure 7: A diagram of the workings of a Scheimpflug [29].

The Illumination System

To be able to capture anything at all there is of course light needed. For high speed applications normal room lighting is not sufficient as the shutter is open for only a tiny fraction of a second it means not enough light can reach the sensor in that time. Therefore a powerful laser is used as a light source to make sure that the particles can be captured on the high speed footage. This laser is even pulsed in synchronization with the shutters of the camera such that the light is even more intense. The laser by itself produces not the right type of beam in the right direction, for this optics are used. These optics consist of a set of focusing lenses, an arm to be able to aim the light, and finally a diverging lens in order for the light to cover the whole measurement area. Finally it is important that both the laser and the four cameras are synced up since otherwise either not the same moment in time would be captured or it would be dark and nothing would be captured. This is done using a device that makes sure these components synchronized.

The Bubble Generator System

The particles themselves are created by the bubble generator, this system consists of mostly 2 parts, with the first one being the device that makes the right mixture for the soap bubbles. This device is called the Helium Filled Soap Bubbles (HFSB) in the case of the Lavision system. Together, air, helium, water, and soap are mixed to create the right mixture. This mixture you can adjust by adjusting the pressures of the helium and or the air. Then the mixture is fed towards the nozzle profiles which are located inside of the wind tunnel. These nozzle profiles are symmetrical airfoils with small holes in the trailing edge, this is done to disturb the airflow as little as possible while being able to inject very precisely sized helium bubbles in the air. These helium filled soap bubbles are all within a certain size which is also important later for the software to be able to recognize them. Lastly the mixture is made such that the bubbles are neutrally buoyant which is important for them not to be under any other forces then the airflow acting upon them.

The Software

Last but not least is the software side of the PTV setup. The three systems discussed until now are technically enough to capture the data necessary, however the footage captured is rather useless without the right data processing and analysis. This process starts with the calibration of the setup and this is done in two steps. First the calibration plate is needed to calibrate the cameras and for the software to know their relative locations to the measurement area in which the calibration plate is placed. Although this kind of calibration would normally be enough for measuring with four cameras, in this case due to the high seeding, that being the number of particles per volume, used in the experiments using only this method is not accurate enough. This is because of an array of small errors that could occur such as mechanical instabilities of the camera setup or inaccurate calibration plate movement [30]. Because of this a volume self calibration has been developed by Wieneke et al. [30] which is used to improve the disparity between the cameras and is the second step in the calibration process.

In order to find the particles themselves after one of the measurements they could just be triangulated, but a faster and more accurate method has been developed by Schanz et al. [31] The method is called shake-the-box and it comes down to instead of triangulating the particles in each time step and afterwards determining the velocity of the particles, they use the velocity data of the particle to estimate an area where it most likely will be in the next time step. This estimation already gives a location to search for the particle in the next time step with a relatively small error. After tracking the particles that could be tracked they are removed from the data and subsequently the algorithm tries to identify new particles, which, because of the reduction in particle count is now easier and more accurate to do. This method promises virtually no ghost particles if used properly [31].

2.4.2 Divergence Check

Now that there is a way of getting data it is important to check if this data is indeed valid to use. A good way of checking this is to see if the obtained data is indeed incompressible, as was explained in section 2.4, which is done by checking if the divergence is zero. To see what this means we must first take a look at the continuity equation given in 5. This equation is derived from the fact that no mass can either be created or destroyed. Meaning that the mass flow in or out of a control volume is equal to the change in mass of that volume [25], this is expressed in the equation 5.

$$\frac{\delta\rho}{\delta t} + \nabla \cdot \rho V = 0 \quad (5)$$

Where ρ is the density of the fluid, and V is the velocity of the fluid [25].

From this equation and the fact that in an incompressible flow the change in density is equal to 0 and ρ can be substituted out, we get equation 6.

$$\nabla \cdot V = 0 \quad (6)$$

This gives us a very useful check to analyze the data with, and see if the measurements were accurate enough to be used. For example if there were to be many ghost particles or the measurements were done inaccurately this condition would not hold.

2.4.3 Lambda-2 criteria

To be able to see when the LEV exactly detaches from the airfoil it needs to be measured. Since with PTV particles in the airflow can be measured quantitatively, criteria can be used to measure if certain structures exist. For vortices there are multiple characterizations or criteria to determine which parts of an airflow belong to a vortex. Vortices are generally characterized by a swirling motion around a central region, which comes from the intuitive understanding of a vortex. The paper by Jiang et al. [32] goes over various methods of characterizing vortices and compares these methods. Of these methods, the focus will mainly be on the lambda-2 criteria. As proposed by Jeong and Hussain [33] the lambda-2 criteria was proposed due to two effects not being accounted for in other methods. These first part is that unsteady irrotational straining can lead to there being

a pressure minimum without a vortex, and secondly the viscous effects leading to an elimination of the pressure minimum inside a vortex [32].

Instead they propose a different definition that disregards irrotational straining, and viscous effects. They first relate the Hessian of pressure, for which the critical point represents the pressure minimum, to the Navier Stokes equation in the following way:

$$a_{i,j} = -\frac{1}{\rho} p_{,ij} + v u_{i,jkk'} \quad (7)$$

Where p_{ij} is the Hessian of pressure. For there to exist a pressure minimum or critical point, the Hessian matrix requires two eigenvalues to be positive. On this principle the lambda-2 method is based. $a_{i,j}$ is the acceleration gradient, here Jeong and Hussain [33] ignored the terms that stand for the unwanted parts (irrotational straining and viscous effect) and are left with: $S^2 + \Omega^2$ where S^2 is the strain-rate tensor and Ω^2 is the rotation rate tensor. This results in the fact that at least two eigenvalues of the matrix $S^2 + \Omega^2$ need to be negative in order for a pressure minima to exist and thus for the flow to be part of a vortex core. And because $S^2 + \Omega^2$ is symmetric its eigenvalues are only real if $\lambda_1 \geq \lambda_2 \geq \lambda_3$, and thus λ_2 needs to be smaller than 0. The full derivation can be found in the paper by Jeong and Hussain [33].

2.4.4 Corrections

Testing airfoils in a wind tunnel is a very useful way of getting information, but it is of course never the ideal world. Compensations need to be done to correct the data and be able to use and compare the results with each other.

Blockage Correction

Blockage correction is needed because, with a large enough airfoil, a restriction is created which leads to a pressure drop that can influence the results. To see if blockage correction is necessary the blockage ratio is calculated. It is defined as the frontal area of the test piece divided by the total cross sectional area of the test section. For there to be a negligible influence of the blockage effect by the test piece, the blockage ratio should be under the 5%. For this case no blockage correction is necessary. For items or angle of attacks with a blockage ratio higher than 5% a blockage correction is necessary. As will become clear in section 3 the configuration with the largest blockage ratio for the experiments done was a blockage ratio of 21%. Typically blockage ratios do not go much higher than 10% to 15%, however blockage corrections have been successful even up to ratios of 20% to 30% blockage [34].

The blockage effect is caused by two separate effects called the solid blockage and the wake blockage. The solid blockage is the effect of the air increasing in velocity around the model since the model creates a smaller space to get through. This can be deduced by continuity and Bernoulli's equation. [34]

The wake blockage on the other hand is the effect of the test piece creating a wake. The flow velocity in this wake is lower than the incoming air before it hits the model. Bernoulli's principle states that an increase in flow velocity causes a drop in the air pressure. For this reason a pressure gradient and flow velocity gradient exist around the model, which need to be compensated to get an accurate result.

These effects have been modelled and from this model the following compensation is obtained. First in order to correct the velocity, angle of attack, lift coefficient, pitching moment, and drag coefficient a compensation factor must be known. In equation 8 the total blockage compensation factor is given, which consist of, as explained before, of the solid blockage and the wake blockage.

$$\epsilon = \epsilon_{sb} + \epsilon_{wb} \quad (8)$$

The two parts are then calculated as follows in equation 9 and 10 [34].

$$\epsilon_{sb} = \Lambda * \sigma \quad (9)$$

This is the equation for solid blockage, Where Λ is a factor depending on the shape of the profile, and σ is a factor depending on the relative size of the airfoil versus the tunnel. [35].

$$\epsilon_{wb} = \frac{c/h}{2} * c_{du} \quad (10)$$

This is the equation for wake blockage as suggested by Maskel [36]. Where c/h is the relation of the chord length versus the tunnel height, and c_{du} is the uncorrected drag coefficient.

From equation 9, Λ is dependent in a complex way on the size and shape of the profile that is being tested [35]. On the other hand Pope uses the following definition $\Lambda = 4\lambda_2 t^2/c^2$ where λ_2 (not to be confused with the lambda-2 criteria) contains the properties of the given airfoil. For λ_2 , values have been determined experimentally. [34].

σ on the other hand only contains information about the relation of the wind tunnel and both Pope et al. [34] and Allen et al. [35] agree that it is defined as $\sigma = \frac{\pi^2}{48} (\frac{c}{h})^2$.

Finally this correction factor ϵ can now be used to calculate the corrected lift coefficient, next to this a corrected angle of attack needs to be calculated.

$$\alpha = \alpha_u + \frac{57.3\sigma}{2\pi} (c_{lu} + 4c_{m\frac{1}{4}u}) \quad (11)$$

Where α is the (in this case) corrected angle of attack, u indicates uncorrected, and $c_{m\frac{1}{4}m}$ is the uncorrected pitching moment around the quarter chord.

$$c_l = c_{lu}(1 - \sigma - 2\epsilon) \quad (12)$$

Where c_l is the (in this case) corrected coefficient of lift, the subscript u indicates uncorrected, and σ and ϵ were described earlier.

Weight Correction

Because gravity is pulling down on the airfoil at different angles during the experiment it needs to be taken into account. The correction is rather straight forward, for example when the weight of the test piece is known its force on the load cell under every angle could be calculated and subtracted from the result. A different route was chosen however. With the wind tunnel off the test piece was measured at every angle that was measured at. This meant that the exact load cell values for only the weight off the test piece were measured and could later be subtracted from the results. The reason for the choice to do it this way was for it to be deemed more accurate, for example because the angle indicator on the wind tunnel does not give angle relative to gravity but angle relative to the wind direction.

2.4.5 Force Balance

In the smaller of the two wind tunnels a force balance is used to measure the force on the airfoil. The exact force balance present in the Educational Wind Tunnel (EWT) can be seen in Figure 8. When measuring the force on an object there are several ways of doing so. The use of a strain gauge is one of the more common ways and is generally a rather versatile way of doing so. In case of the

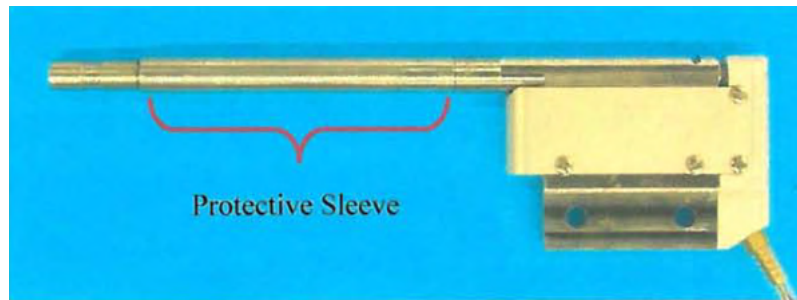


Figure 8: *The stinger as can be found on the EWT, gotten from the EWT Manual [37].*

EWT a stinger type force balance is used. The strain gauges in the case of this stinger are under the protective sleeve, most wires are very thin so need to be protected from the model that gets attached to this stinger. The load cell measures forces in 3 Degree Of Freedom (DOF). Normal, Axial, and Pitching. by rotating the stinger axially by 90 degrees a side force and yawing moment can be measured instead of normal and pitching. More information about the specific setup for the wind tunnels that were used can be found in section 3.

3 Method and Approach

This section discusses the methods used in this research. Furthermore it explains the experiments done and their setup, making it clear exactly how these experiments were conducted. Two experiments were done, namely: static wind tunnel testing using a load cell on an airfoil, and dynamic wind tunnel testing using the PTV setup on the RoBird wing. The dynamic refers to the wing and whether it is flapping or stationary.

First the experiments which were done in the smaller of the two wind tunnels will be discussed. Eventually with the information gained from these experiments the dynamic experiments in the larger wind tunnel were conducted which is described later in this section. It is important to note an assumption was made between these two sets of experiments. Namely the assumption that the flaps that seem to have more influence in the static case will also work best in the dynamic case. This was taken as a starting point as almost non of the literature covers the dynamic case.

3.1 Static Testing Using a Load Cell on an Airfoil

It must first be understood how the design of the covert feathers influence the airflow and thus force on an airfoil. For this reason static experiments were conducted in the smaller wind tunnel, on the basis of a research paper by Izquierdo et al. [10] as covered in section 1.4. The design variables of these flaps were changed accordingly in order to confirm which flap showed the best results. Later it was decided to change other variables too since it was clear that variables not discussed in the paper were also very influential, such as the length of the flaps. In this section the setup and methods used to find an answer to the second research question will be discussed in parts. Starting with the wind tunnel, then the airfoil used, the flaps and what was changed about them, the measurement conditions, and finally how the data was processed and analyzed

3.1.1 The Wind Tunnel

The setup for this experiment will of course be very similar to the setup as described in the paper. The main difference is the wind tunnel. The wind tunnel used in the setup for this experiment is made by Aerolab and is called the Educational Wind Tunnel (EWT) [37]. The test section of this wind tunnel is 305 x 305 x 610 mm big and the sides are made of acrylic sheets so that the test piece can be observed well. The wind is produced by a 7.5kW electric motor which is controlled using a VFD which itself can be controlled either manually or by a feedback loop that measures the wind velocity.



Figure 9: Image of the setup with the 3D printed airfoil on the stinger balance of the small wind tunnel with one of the laser cut flaps installed.

For capturing the data a national instruments device was used that comes inside of the wind tunnel, this logs among other information the forces on the force balance, the wind speed, the angle of attack and it gives some control inputs for the wind tunnel. The force balance is of the stinger kind and is discussed in more detail in section 2.4.5. The data is captured via the computer connected to the national instruments device and by clicking on a "Take Data" button these values are saved in a csv file, when clicking another time this would add an entry to the same csv file. Since the values of the load cell were not fully stable an average was taken of 100 samples by using an auto clicker on the "Take Data" button.

3.1.2 The Airfoil

Expect for the difference in length of the paper flaps, everything has been done in the same conditions as the experiment in the paper by Izquierdo et al. [10]. This means that the airfoil that was used was the SD 7003, this is a slightly cambered airfoil and has a max cl of about 1.2 after which it stalls at an angle of attack of about 12° [38]. This airfoil was 3D printed using a Prusa i3 MK3S using PLA material. The design was made in solid works to be able to add the mount that could attach to the stinger of the force balance in the wind tunnel. The wing was designed to be 285 mm wide such that it would fit wall to wall without touching the sides of the wind tunnel. The chord length was first taken to be the same as in the paper: namely 196 mm. However it was found that this caused too much blockage in the wind tunnel, it was then decided to change this to half the size, and by doubling the wind speed to 26.3 ms^{-1} keeping the Reynolds number the same at 170 000

3.1.3 The Flaps or BICF's

The flaps, or Biologically Inspired Covert Feather (BICF) as the paper calls them, were made based on the paper however just like the airfoil scaled down to half the size. Instead of BICF more intuitive terms will be used to describe the various shapes of the flaps. These flaps were cut from paper using a Trotec laser cutter. This method proved to be very useful since for almost each individual test in table 1 a different sized or shaped flap needed to be made. The laser cutter made this a very painless process. The paper that was used was standard 80 g A4 paper, and for the larger ones 80 g A3 was used. The flaps were attached to the airfoil using electrical tape, and was only applied on the strip at the base of the paper flaps where they were connected to each other.

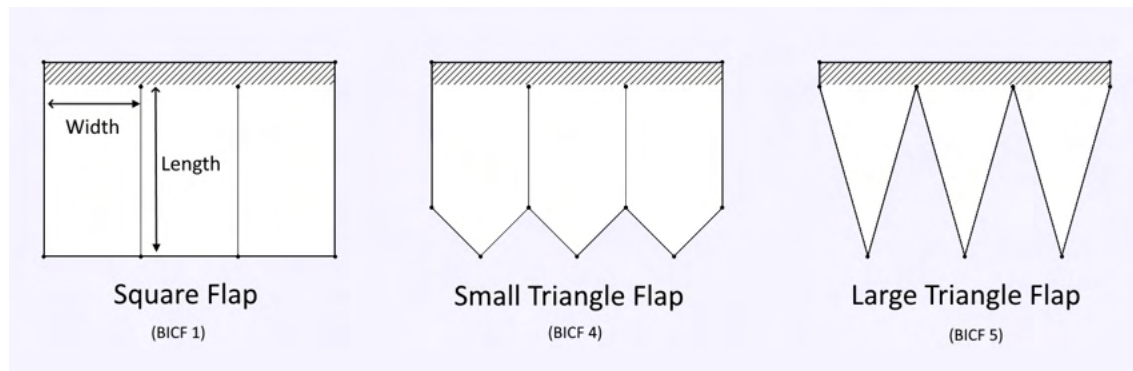


Figure 10: The shapes used for the paper flaps with their respective names (including the names as described by Izquierdo et al. [10]). The large triangle flap design has been added. The greyed out area is where the tape was attached. The width and length mentioned in the table is the width and length as can be seen in this figure.

3.1.4 The Measurement Conditions

The experiments that were eventually done overlapped only a little with the paper on which they were based. Instead, also other variables, and in other combinations were changed. An overview of the variables that were decided to change can be found in table 1. The shape and location were changed just as in the paper, but also the length, width, and Reynolds number. Of course a reference case was also measured to be able to see the difference the flaps might make. Everything was eventually setup in such a way that it was easy to change width and the length of the flaps as described in table 1. Because of this it was possible to conduct many experiments.

In the table the experiments are grouped together, this is done to give a better overview over which variable was changed within that group. The order in the table is however also the chronological

Experiment	Shape	Length [mm]	Width [mm]	Location [chord]	Reynolds Number	Comments
0	N/A	N/A	N/A	N/A	174,000	Reference Case
1	BICF 1	10	10	1/4	174,000	
2	BICF 4	10	10	1/4	174,000	Changed Tape
3	BICF 4	10	10	1/4	174,000	Changed Tape
4	BICF 4	10	10	1/4	174,000	Changed Tape
5	BICF 1	20	10	1/4	174,000	
6	BICF 1	32.5	10	1/4	174,000	
7	BICF 1	45	10	1/4	174,000	
8	BICF 1	32.5	10	1/4	174,000	
9	BICF 4	32.5	10	1/4	174,000	
10	BICF 5	32.5	10	1/4	174,000	
11	BICF 1	32.5	20	1/4	174,000	
12	BICF 4	32.5	20	1/4	174,000	
13	BICF 5	32.5	20	1/4	174,000	
14	BICF 4	10	10	1/4	174,000	
15	BICF 4	10	10	3/4	174,000	
16	BICF 4	32,5	10	3/4	174,000	
17	N/A	N/A	N/A	N/A	99,000	Reference Case
18	BICF 1	10	10	1/4	99,000	
19	BICF 4	32.5	10	1/4	99,000	
20	BICF 5	32.5	10	1/4	99,000	
21	BICF 1 & 4	32.5 & 10	10	1/4 and 3/4	174,000	double flaps

Table 1: *Table of the variables changed during the experiments done in the small wind tunnel, the width, length and shape can be found in figure 10*

order in which the experiments were conducted. Experiment 0 was the reference case without any flaps. In the second group of experiments there is one experiment that has been done 3 times. This was due to complications with the tape letting go which is discussed in more detail in section 5. For experiment 5, 6, and 7 the length of the flaps was changed. For experiment 8 - 13 the shape (including width) was changed. For experiment 14, 15, and 16 the location was changed. Experiment 17 - 20 was a comparison for various setups while testing at a different Reynolds number. Finally the last experiment was done with double flaps, this was compared to previous experiments as can be seen in the result section.

3.1.5 Data Processing & Visualization

In order to quickly analyze the data matlab R2021b was used to create a script that imports the data from the wind tunnel. After this data was imported the script would convert the wind tunnel sensor data to the lift coefficient and calculate and propagate the corresponding errors. After the uncorrected lift coefficient had been calculated, the blockage correction was done and then the weight correction. Finally this corrected data together with its error is plotted in a figure. The script was made in such a way the user can select which files should be compared to each other, these are then plotted in the same graph for an easy comparison. Variables such as the Reynolds number and kinematic viscosity were filled in manually before the script was run. The script uses a separate file containing the data for the weight correction of the specific airfoil used as described in section 2.4.4. The file is automatically loaded into the script and used. For a more detailed explanation about the exact corrections that were done see section 2.4.4.

3.2 Dynamic Testing Using the PTV Setup on the RoBird Wing

In order to get a better understanding of the working of the upper covert feather flaps and their influence on the flight characteristics, experiments were done in the large wind tunnel using the PTV setup available there. The working of the PTV setup is explained in section 2.4.1, however the exact system which is used in the wind tunnel at the University of Twente is discussed in this section. Furthermore this section will focus on the other parts of the setup such as the wing itself and the flapper mechanism. Finally it will be explained how the data was gathered, processed, and analyzed.

3.2.1 The Wind Tunnel

The large wind tunnel of the University of Twente is used for this experiment as the test section is big enough to house the RoBird wing. The test section of the wind tunnel consists of the 700 mm × 900 mm rectangle which opens up into a large acoustic room. The size the room itself is 6 m × 6 m × 4 m. Behind the square frame of the closed test section another frame has been made to which various test pieces can be fitted. Two large toothed roller bearings are part of this frame such that the test piece can be set under any angle of attack, these can be seen in Figure 11a and are surrounded by the yellow tape. Either the closed or half open part of the test section can be used. For the latter one the top and bottom are still closed but the sides are open. The top and bottom need to stay closed because this is where the roller bearings are and the test piece is fitted to. In Figure 12a a test piece can be fitted to the roller bearings. The wind tunnel uses two large radial wind turbines connected to a 130kW electrical motor. This makes it possible to reach wind speeds of up to 60 m s⁻¹, which is also more than enough range for these experiments [39].

3.2.2 The PTV Setup

In this section the specifics of the PTV setup that was used are discussed. For the whole system to function numerous parts are necessary that need to work together as one system. Similarly as the theory section 2.4.1 the setup will be discussed in four parts. The processing and analysis is in this case the software part which is discussed at the end of this section.



(a) *The arm with laser optics of the illumination system.*



(b) *The four Phantom slow motion cameras used for capturing the data.*

Figure 11: *Parts of the illumination system and the capture system.*

The Capture System

For the capture system 4 phantom high speed cameras were used, 2 of these were the Veo model and 2 of them were the older V611 model. This made for a slight difference in the setting up of these cameras however it did not make a difference for any of the results. One of the more

important things that needed to be payed attention to, was the sturdiness of the camera frame. Since the cameras are not allowed to move especially not relative to each other, as this would cause accuracy problems after the camera calibration had been done. A camera with a recording speed of 2000 Hz was used. The cameras needed to be equipped with the according scheinpflug which lavision supplied with the cameras.

The Illumination System

For light source a Photonics dual-cavity laser was used. This laser is of the ND:YAG type and has a wave length of 532 nm Due to a problem with the previous laser a new one was sent and came in just on time. For the optics lenses were used and an optical arm (as can be seen in Figure 11a) to transport the light to the right location after which it is diverged through a lens such that the whole measurement area is well lit. In order to focus the laser it was turned on a very low power setting and using plates that show the laser light the beam was focused at as far of a distance possible within the actual wind tunnel chamber. After that the arm was placed and aligned such as much of the laser light as possible reached the exit of the arm. It then only needed to be aimed at where the measurement area was, again using reflective tape that actually made the light visible. Since this type of laser is not very efficient when it comes to the power needed to obtain the laser light necessary for the measurements, the excess heat needs to be cooled. For this a large chiller is used. The chiller sits outside of the wind tunnel and tubes, one for hot and one for cold water, are used to transport the heat and water cool the laser. The cooling system is filled with demineralized water and anti rusting agent for the insides of all the components not to corrode.

The Bubble Generator System

The Bubble generating system consisted of multiple parts, namely the HFSB, the nozzle profiles, helium, compressed air, and soap. With the HFSB in the middle, its job is to combine these liquids and gasses in such a mixture that a specific and consistent stream of soap bubbles is formed at the nozzles in the wind tunnel. These bubbles are partially filled with the helium for them to become neutrally buoyant and thus are not influenced by gravity. The mixture before it is blown out of the nozzles goes through an umbilical cord towards all the nozzle profiles that are standing in the wind tunnel. The wind of the wind tunnel is what makes the bubbles move away from the nozzles, otherwise they would just float around. The HFSB in this way can make bubbles down to 300 μm at 1300 bubbles per centimeter cubed at the nozzle exit [40].

The Safety System

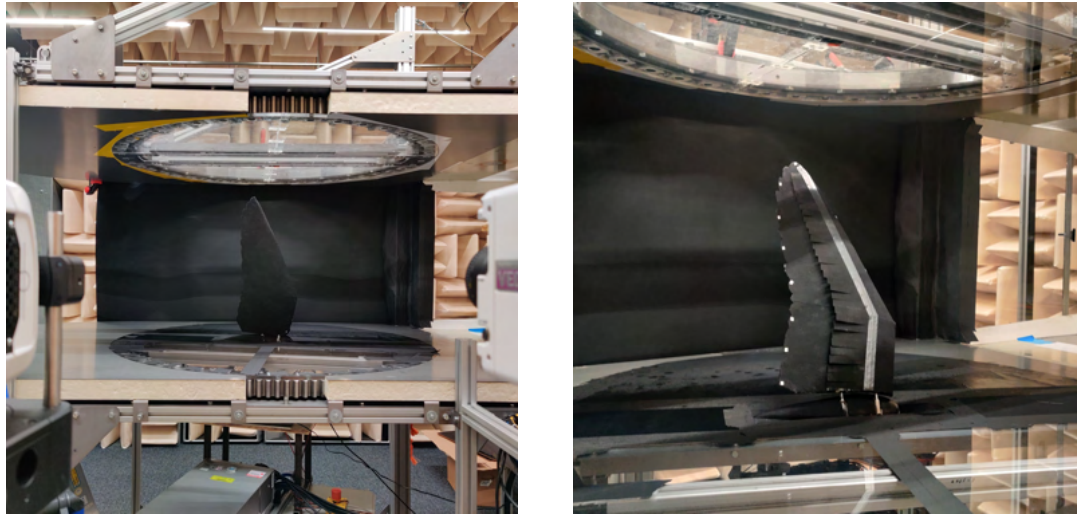
Last but not least there were some systems in place to make sure everything worked properly and safely, first of all, all of the cameras together with the laser needed to be synchronized for the cameras to know when to open the shutter. This was taken care of by the Programmable Timing Unit (PTU). All of the cameras and the laser connected to this device, also including the flapping mechanism to know when the mechanism was at its zero position.

Secondly there was the safety system, this system was developed by the people at the wind tunnel and is made for this specific setup. It connects all the devices, alarms, door switches, lights, and safety features together such that the system only operates under the condition that all the safety conditions are met. When calibrating the laser for example we needed to be in the room with the laser which was possible due to the correct laser safety goggles that were available.

3.2.3 The Wing & Flaps

A total of 2 wings were used during these experiments. These wings were not specifically manufactured for the research done in this paper, but where instead used from the actual RoBird itself. Multiple wings were available and a couple were already painted matt black for PIV or PTV Testing. This is necessary for the intense laser light to not reflect on anything that is visible to the cameras in the background. Regular matte black from a spray can was tried before, however it was found a special paint was necessary to make the wing and the flaps not reflect too much laser light. This paint was Black 3.0 and is based on the somewhat popular vanta black.

These were the two wings that were used of which one was fitted with the covert feather flap design on which was decided by the first experiment. This wing can be seen in the flapping mechanism in Figure 12b. To one of the wings the covert inspired flaps are attached. The flap that was attached was the square shaped flap or BICF 1 at a length of 32.5 mm and a width of 10 mm at a location of $\frac{1}{4}$ chord length. This flap was found to be the most effective in the previous experiments. In order to scale this up to the actual RoBird wing size, all these values were scaled according to the relative wing size.



(a) Picture of the wing from the point of view of the high speed cameras.

(b) Picture of the wing installed with the aerodynamic flaps attached.

Figure 12

3.2.4 Flapping Mechanism

One of the more custom parts of the entire setup is the flapping mechanism. In order for the wing to make a bird like flapping motion this mechanism is used which was developed earlier at the Robotics and Mechatronics (RaM) research group at the University of Twente. The purpose being: be able to flap one of the RoBird wings in the wind tunnel at several angles of attack and several flapping frequencies.

One of the biggest limits of this specific mechanisms is its maximum flapping frequency. This flapping frequency is limited by the motors and their drivers as they simply can not handle more power. The maximum flapping frequency of this mechanism is therefore only 3Hz. To obtain this frequency the drivers are supplied with a voltage of 30 V instead of their rated 24 V.

Another limit of this device is the way it flaps the RoBird wing. An improved flapping mechanism is also being developed at RaM. The goal of this improved mechanism is to overcome exactly these limits. The flapping frequency limit of the improved setup should be around 10 Hz, and furthermore it has an extra degree of freedom. This extra degree of freedom is the rotation or angle of attack of the wing, and it will be able to change this during the flapping motion (unlike rotating the whole mechanism to increase angle of attack). This makes it possible to simulate more complex and accurate wing movements. The improved setup should be able to measure the forces on the robotic bird wing while flapping. It will have a 6-DOF force sensor attached to the base of the wing. Through this force sensor a lot more information and insights could be obtained is maybe the biggest perk of the improved setup. you will have data from not only PTV but you can compare this to the data of the force sensor. which could give a lot more insight.

3.2.5 The Measurement Conditions

The different conditions and variables as were used in the experiments are described below. The values that were kept constant (as a function of the airspeed) are not shown in the table but were as follows: The Reynolds number was 79 167, 105 556 and 131 945 for 6 m s^{-1} , 8 m s^{-1} and 10 m s^{-1} respectively. The flapping frequency was 3 Hz, the flapping amplitude was 0.63 m, and the Strouhal number was 0.315, 0.236 and 0.189 for 6 m s^{-1} , 8 m s^{-1} and 10 m s^{-1} respectively. Some other variables that were played with but mostly stayed constant were for example the Helium and air-mixture values. However these were kept constant by the technician such that the performance was that what was desired. Each of the experiments in the table below consist of 5 cycles, meaning 5 wing beats. This is done in order to obtain more data and be able to take the average of 5 cycles.

Experiment #	Wind Speed [m/s]	AoA [deg]	Flaps [yes / no]	Location	Comments
1	6	10	yes	Downstroke	Not great data
2	8	10	yes	Downstroke	Not great data
3	10	10	yes	Downstroke	Not great data
4	6	20	yes	Downstroke	Not great data
5	8	20	yes	Downstroke	Not great data
6	10	20	yes	Downstroke	Not great data
7	6	10	no	Downstroke	
8	6	0	yes	Downstroke	
9	8	0	yes	Downstroke	
10	10	0	yes	Downstroke	
11	6	10	yes	Downstroke	
12	8	10	yes	Downstroke	
13	10	10	yes	Downstroke	
14	6	20	yes	Downstroke	Used for results
15	8	20	yes	Downstroke	
16	10	20	yes	Downstroke	
17	6	10	no	Downstroke	
18	10	10	no	Downstroke	
19	6	20	no	Downstroke	Used for results
20	8	20	no	Downstroke	
21	6	20	yes	Upstroke	
22	8	20	yes	Upstroke	
23	6	20	yes	Upstroke	No Flapping
24	8	20	yes	Upstroke	No Flapping
25	6	20	no	Upstroke	
26	6	20	no	Upstroke	
27	6	20	no	Upstroke	No Flapping
28	8	20	no	Upstroke	
29	10	20	no	Upstroke	No Flapping

Table 2: Measurement conditions for the experiments done using the PTV setup.

3.2.6 Data Processing & Visualization

The steps done to process and visualize the data were done using the DaVis. This program is part of the PTV setup and has all the necessary tools to plot the data as desired. Multiple processing steps were taken which will be discussed in order. First for all the individual frames a minimum is subtracted such that background noise and other objects in the background are filtered out this also improves the contrast between the bubbles and background. The second step is based on the experience of someone who has worked with this specific setup before. The step consists of a number of image pre-processing steps. The steps until now are done to improve the shake-the-box algorithm and be able to track more particles. The shake-the-box-algorithm is the third step as the particles now need to be tracked. This step takes the most processing time and for multiple data sets can take easily a day to complete. For this reason it was made sure in small batches that the pre-processing was done correctly. Finally a vector field can be generated from the tracked particles, since this is based on the particle tracks, it also means that if there are only a few particles in a certain volume the uncertainty for that volume will be larger.

For the results as can be seen in section 4 all of the 5 cycles were combined and the average was taken of these vector field. DaVis has a tool to calculate and plot the lambda-2 criteria based on the a vector field. This was used to obtain the data. This data was then analyzed and the down stroke portion was exported in six frames. Each of these frames 20 frames apart or 100 ms. Between the two different experiment the frames were synchronized by taking a visual reference point on the wing and aligning that with the same pixel on one of the cameras. Because the system is very susceptible to vibrations or movement of the camera extra care was already taken into not making that happen. Because of that fact this method was accurate.

4 Results

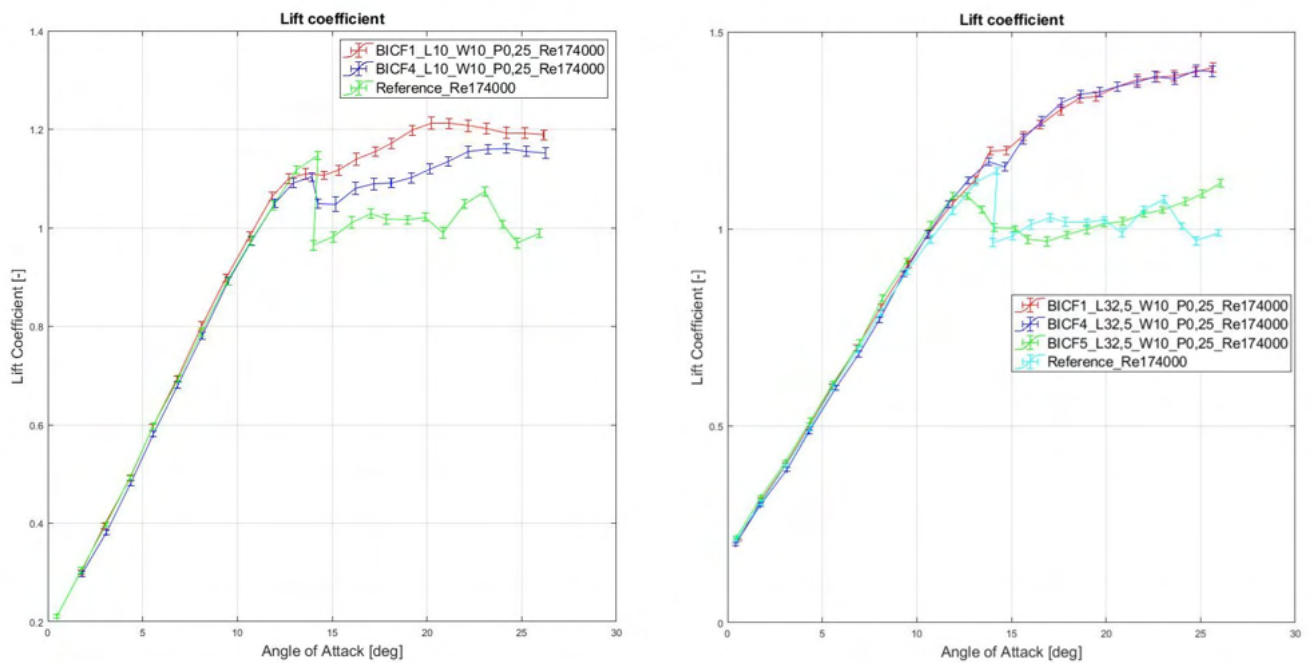
4.1 Static Testing Using a Load Cell on an Airfoil

Based on the experiment table 1 in section 3.1 data will be presented in several plots. Next to that the observations done during the experiments will be presented. In all the following graphs the legend is made up of information about the test in the following way:

[Shape]-[Length]-[Width]-[Place]-[Reynolds Number].

4.1.1 Different Flap Shapes

For the experiments with different flap shapes multiple experiments from other sets in table 1 were used. The first experiment done in the small wind tunnel was with 2 different flap designs and the reference case. Later for flaps with a different length another shape was added, This is presented in the following two graphs.



(a) The lift slope of the SD7003 airfoil with differently shaped flaps attached at a length of 10mm.

(b) The lift slope of the SD7003 airfoil with differently shaped flaps attached at a length of 32,5mm.

Figure 13

4.1.2 Different Flap Lengths

Four different lengths are represented in this graph, together with the reference case. This entire experiment was executed twice, as can be seen by the double lines per colour (or flap length). The flap lengths are 10 mm, 20 mm, 32.5 mm and 45 mm.

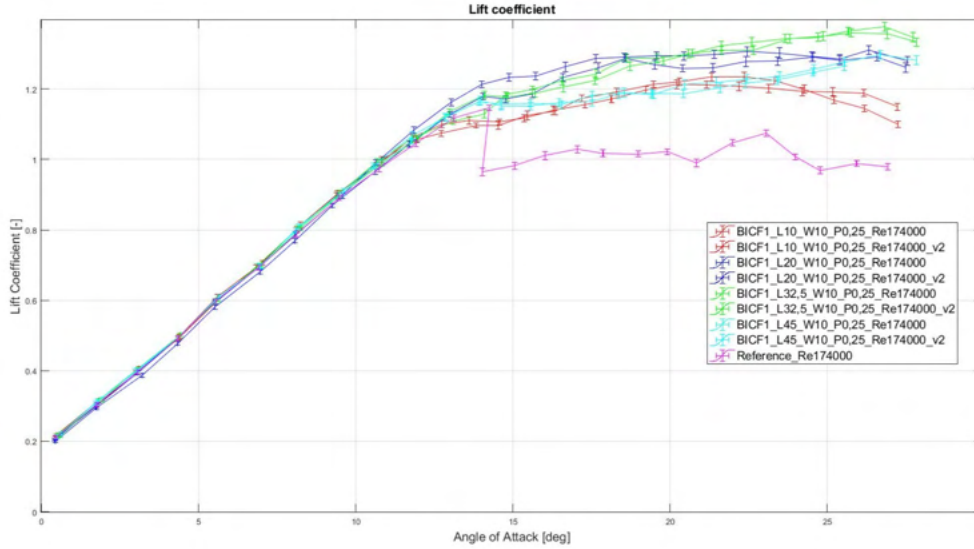


Figure 14: The lift slope of the SD7003 airfoil with different length flaps attached to its top side.

4.1.3 Different Flap Locations

The small triangle flaps at length 32.5 mm were tested at $\frac{1}{4}$ chord length and at $\frac{3}{4}$ chord length. Also the square flaps were tested at $\frac{3}{4}$ chord length.

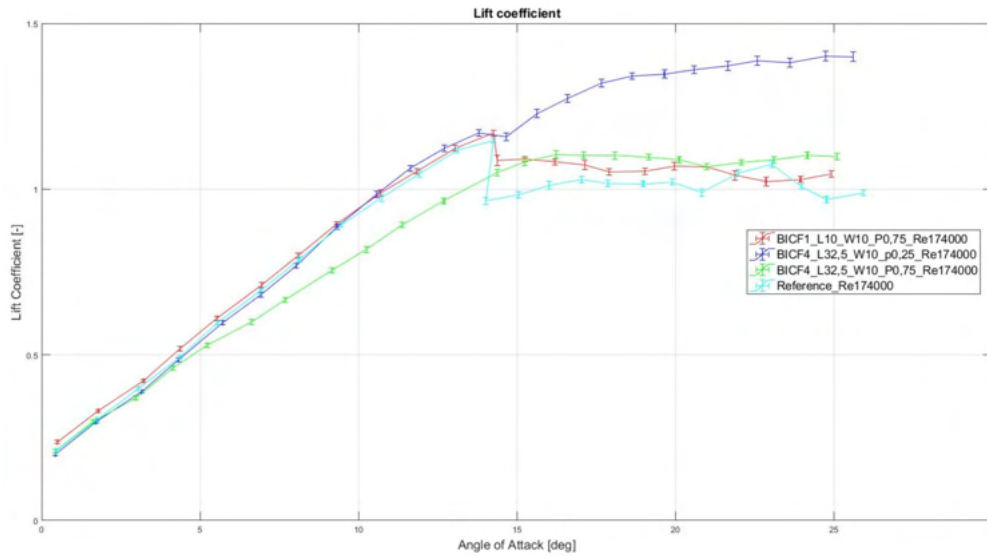
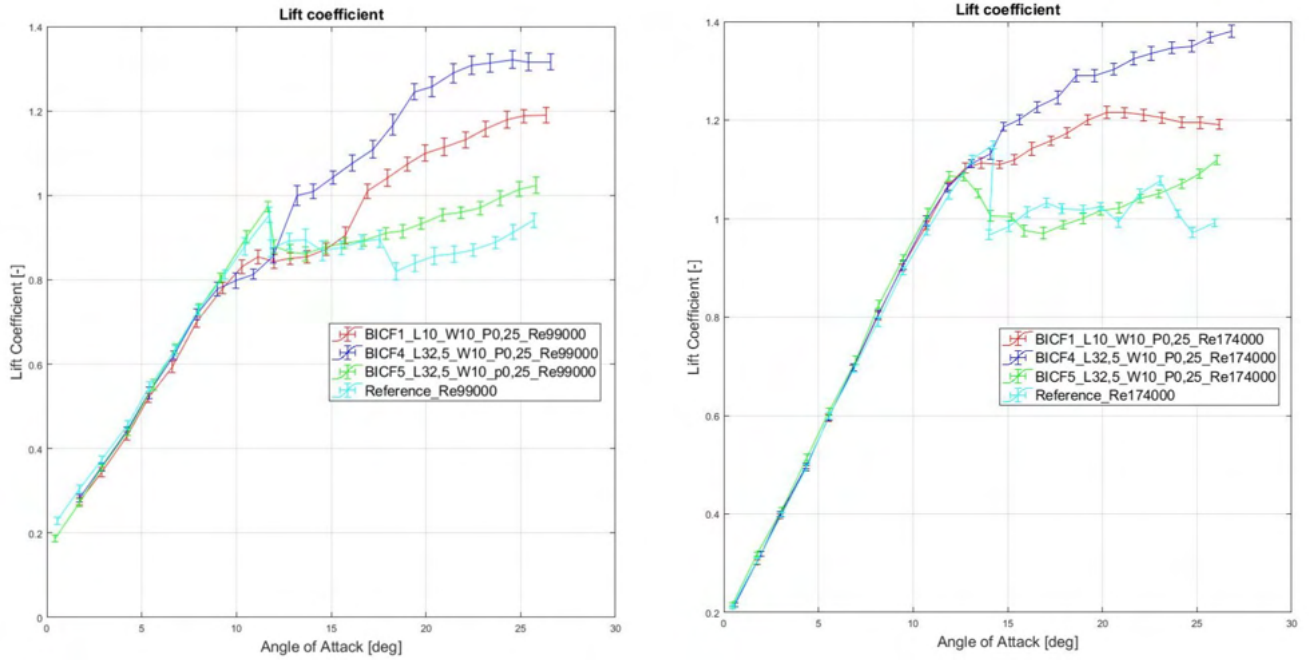


Figure 15: The lift slope of the SD7003 airfoil with flaps attached to its top side in different locations.

4.1.4 Different Reynolds Numbers

Next to a Reynolds number of 174 000 which was used for all experiments, a second Reynolds number of 99 000 was tested. Four different setups were used, which can be seen in Figure 16a and 16b. The Reynolds number was changed by changing the wind velocity accordingly.



(a) The lift slope of the SD7003 airfoil for 4 cases with and without flaps at a Reynolds number of 99000.

(b) The lift slope of the SD7003 airfoil for 4 cases with and without flaps at a Reynolds number of 174000.

Figure 16

4.1.5 Double Flaps

In the following plots the results can be seen for the setup with double flaps. The data for both of these flaps individually attached to the wing is also shown. This gives an overview of the improvements of the airfoil with or without these different flaps. The flap setups used for the double case were BICF4 L32,5 W10 P0,25 Re 174000 together with BICF1 L10 W10 P0,75 Re174000 as can also be seen in table 1.

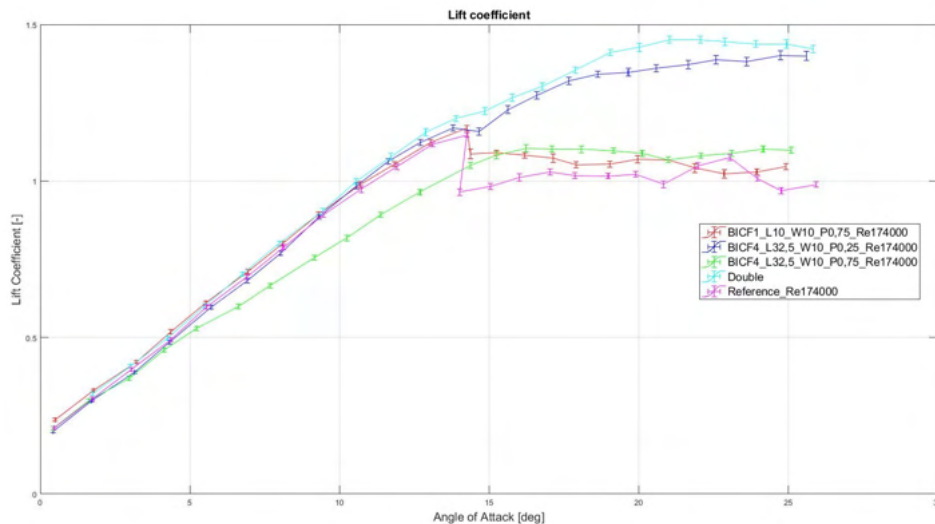
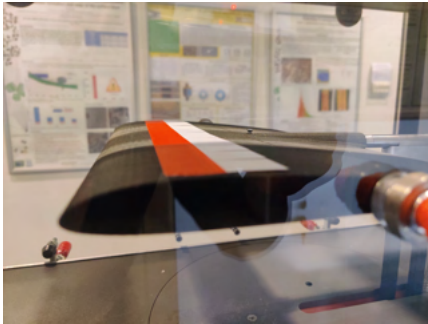


Figure 17: The lift slope of the SD7003 airfoil for different cases including one with 2 different types of flaps attached.

4.1.6 Observations

During the initial testing in the small wind tunnel the airfoil and its flaps were monitored closely, through this many observations have been made. Similar behaviour was observed for almost all flaps, these observations are presented first, after which other more specific observations are presented.



(a) *The large airfoil (198 mm chord length) at a 0° angle of attack*



(b) *The large airfoil (198 mm chord length) at a 13° angle of attack*

Figure 18

General movement of flaps during change in angle of attack:

In most cases the flaps would start flush with the airfoil (as seen in Figure 18a) and then as the angle of attack would increase they would slowly rise up and the angle between flap and foil would become bigger. Then, when getting close to the regular stall angle (around 12°) of the airfoil the flaps would suddenly jump up and transition into a fluttery state where the flaps would move all over. Increasing the angle of attack even further, at some point the flaps would stop fluttering and the angle between the flaps and the airfoil would slowly become larger. In a sense the flaps were not rotating with respect to the airflow even though the airfoil itself was.



(a) *The large airfoil (198 mm chord length) at a 13° angle of attack*



(b) *The large airfoil (198 mm chord length) at a 27° angle of attack*

Figure 19

Span wise distribution:

During the first phase where the flaps moved slowly up a distribution dependent on the span-wise location of the flaps could be seen. This observation is well seen in Figure 18b.

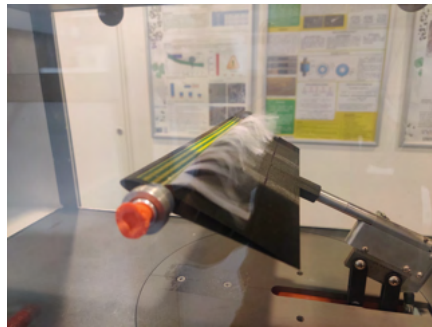
Change in fluttering:

The fluttering that was observed was mostly around the stall angle of the airfoil. From about 8° or 9° until around 15° the movement of the flaps for an increasing angle of attack would be as follows:

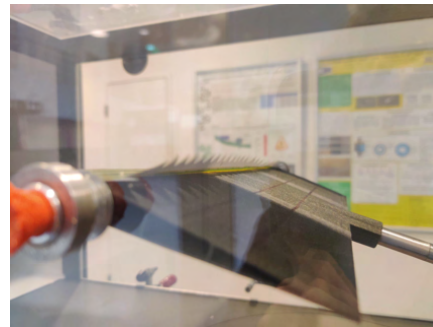
the fluttering would start in small amounts, grow in amplitude and intensity, slowly subside almost to pre-stall levels while bending more and more towards the leading edge of the airfoil. Although in the Figures it is the larger of the two airfoils, these steps / stages described, can be seen throughout Figures 18 and 19.

Transition into fluttering:

The transition from the flaps not moving to fluttering was very sudden. Meaning that (often while increasing the angle of attack) the flaps would sit still and suddenly start to flutter. This transition was for more intense for flaps longer than 20 mm. In these cases the transition could be heard by the sound become louder as the fluttering made noise. Furthermore it could be noticed the fan had to start spinning faster to be able to maintain the same air speed.



(a) *Experiment 7, the small airfoil (98 mm chord length) at a 22° angle of attack*



(b) *Experiment 10, the small airfoil (98 mm chord length) at a 17° angle of attack*

Figure 20

Differences in fluttering:

The amount of fluttering was hard to quantify, but a difference was observed in the amount of fluttering depending on the properties of the flap. First of all the longer flaps would generally flutter more intensely, meaning a larger amplitude and a more chaotic movement compared to the shorter flaps. This is partially shown in Figure 20a by means of the blurriness of the flaps because of their chaotic and fast movement.

Another observation made after measuring the longer flaps was that when the airfoil was turned back to a 0° angle of attack, the flaps would not be fully flush anymore and seemed to be deformed a small amount from the excitation.

Observations for Specific Experiments

Experiment 6

At 6° a slight flutter in the flaps could just be noticed, at 10° the flaps became stable again. Then, at 12° the fluttering became more intense, during which the tape let go quite a bit. Like mentioned before this was one of the cases where the flaps would not be fully flush with the airfoil anymore after the experiment.

Experiment 10

The larger triangles behaved differently than all the square and small triangle flaps. Instead of a clear fluttering motion, barely any fluttering was noticeable and would look very stable. When increasing the angle of attack towards the flaps would also increase their angle between the airfoil and the flaps.

4.2 Dynamic Testing Using the PTV Setup on the RoBird Wing

4.2.1 Footage of Flaps Moving on the Down stroke

In order to get a better idea of how much the flaps are actually deploying during a down stroke, footage was taken without turning on the HFSB so there would be no bubbles. Six exported frames can be seen in Figure 21. Furthermore this footage acts as a reference case when looking at the other graphs, since the same six frames were taken for the other graphs in this section.

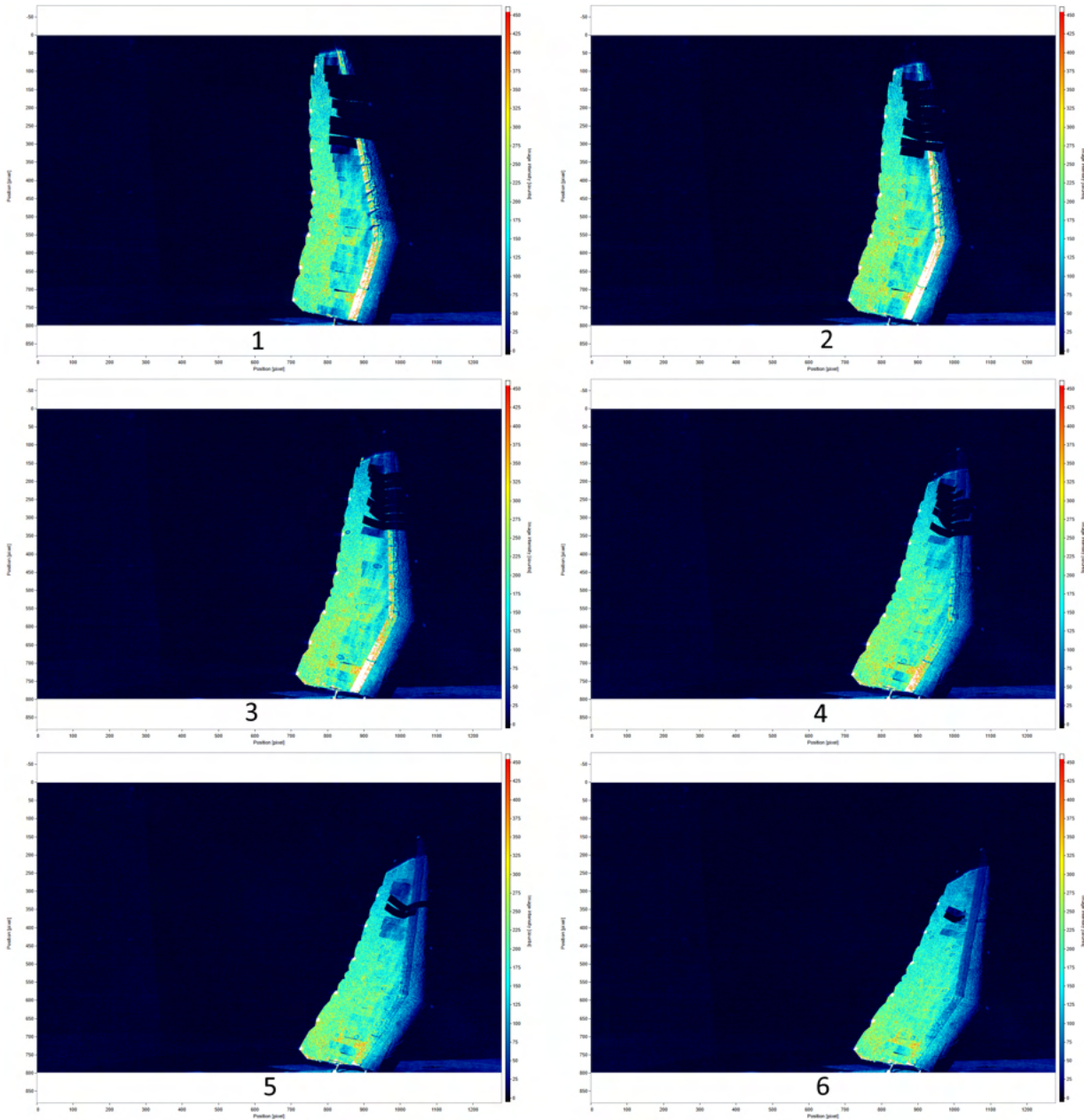


Figure 21: Footage of the wing moving on the down stroke while the flaps deploy mostly at the tip of the wing.

4.2.2 PTV Data of Down Stroke

To give an intuitive insight to what the PTV data looks like, the same six frames have been plotted in Figure 22. This shows the particles that have been tracked in a certain moment of time. The length of the tracks are dependent on plot settings but also on how long the cameras and software were able to track that specific particle.

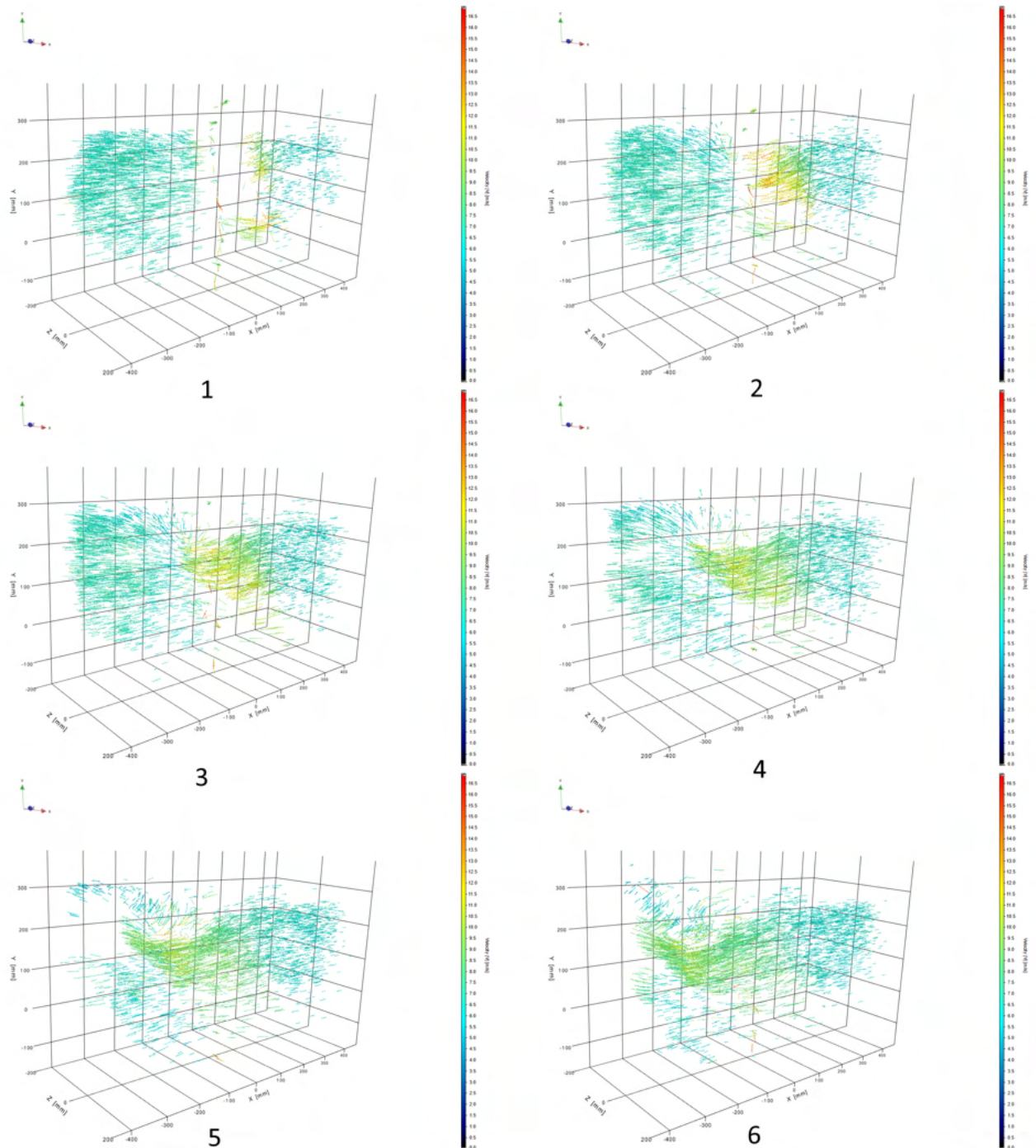


Figure 22: PTV tracks of the measurements with the flaps attached to the wing. The particles are shown as dotted lines with the colour representing the velocity of the particles at their specific place in the measurement space.

4.2.3 Quality of the Data

In the following two images the divergence of two sub planes in the measurement volume has been plotted. The arrows and colour stand for the 3D divergence for those specific voxels, in this case spread over 2 planes. As explained in section 2.4.2 this is a measure for the rate of change in pressure in a certain volume, when this is 0% it means the flow is incompressible.

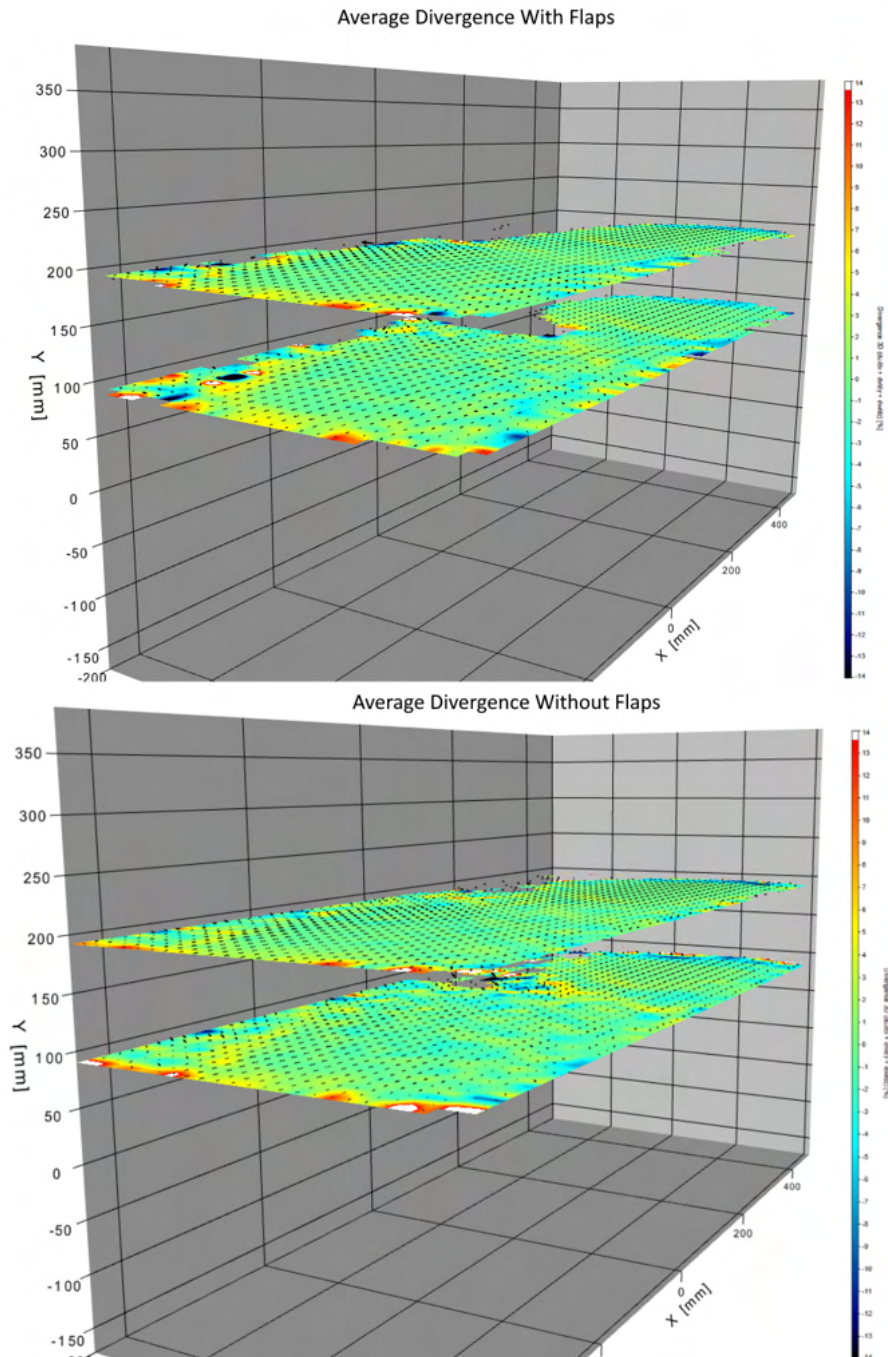


Figure 23: The average divergence of the data for the two shown planes for both the wings with and without flaps.

4.2.4 LEV without and with flaps

Here are six snapshots that are part of all the frames that were captured showing the lambda 2 criteria in the voxel space. Six frames equally spread (every 20 frames) over the moment the wing was on its down stroke and an LEV was created. On the left numbered 1 to 6 are the snapshots for the wing without flaps, and on the right with flaps.

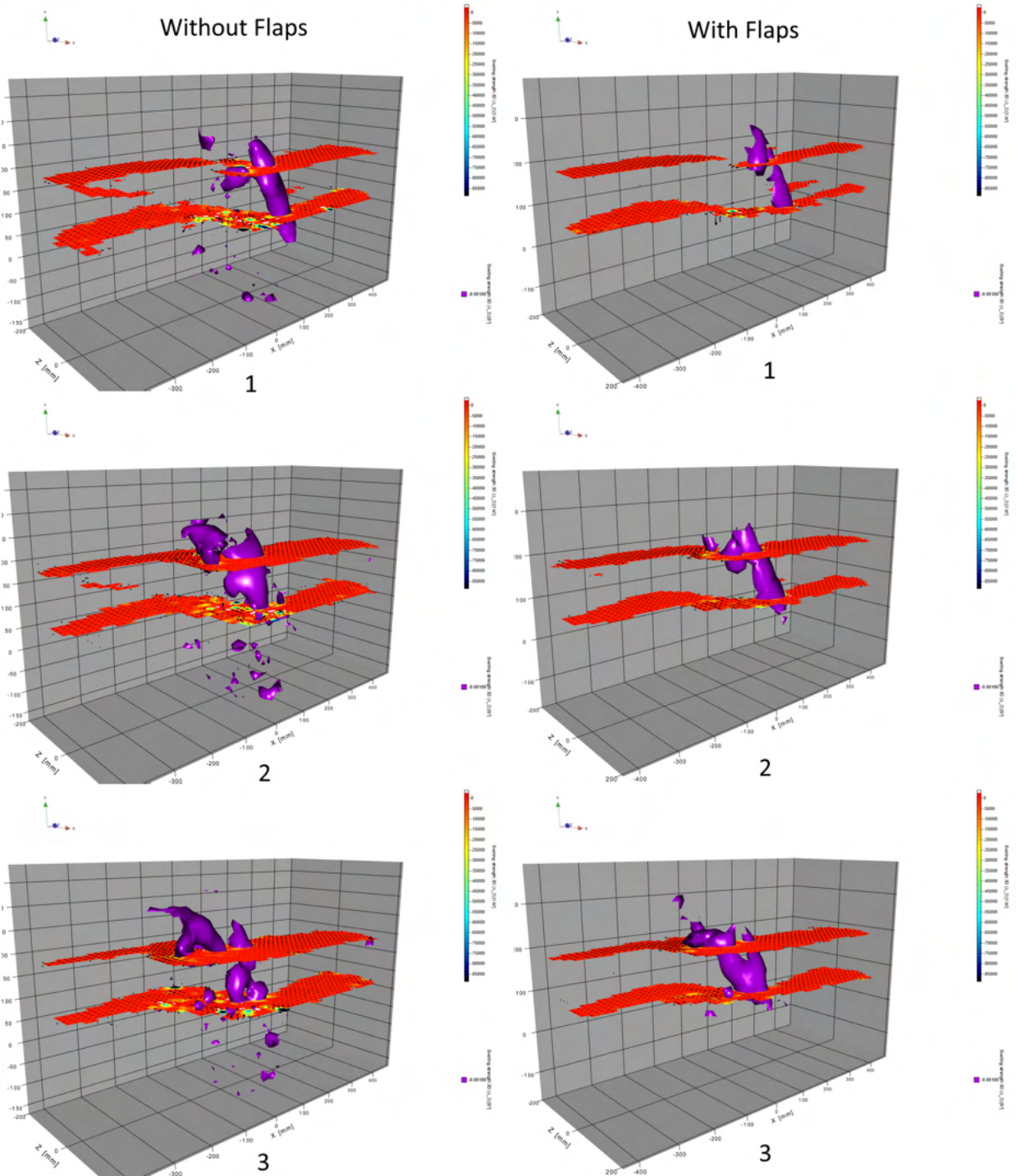


Figure 24: Snapshot 1 to 3 of the lambda 2 criteria data in the voxel space of left without flap and right with flap.

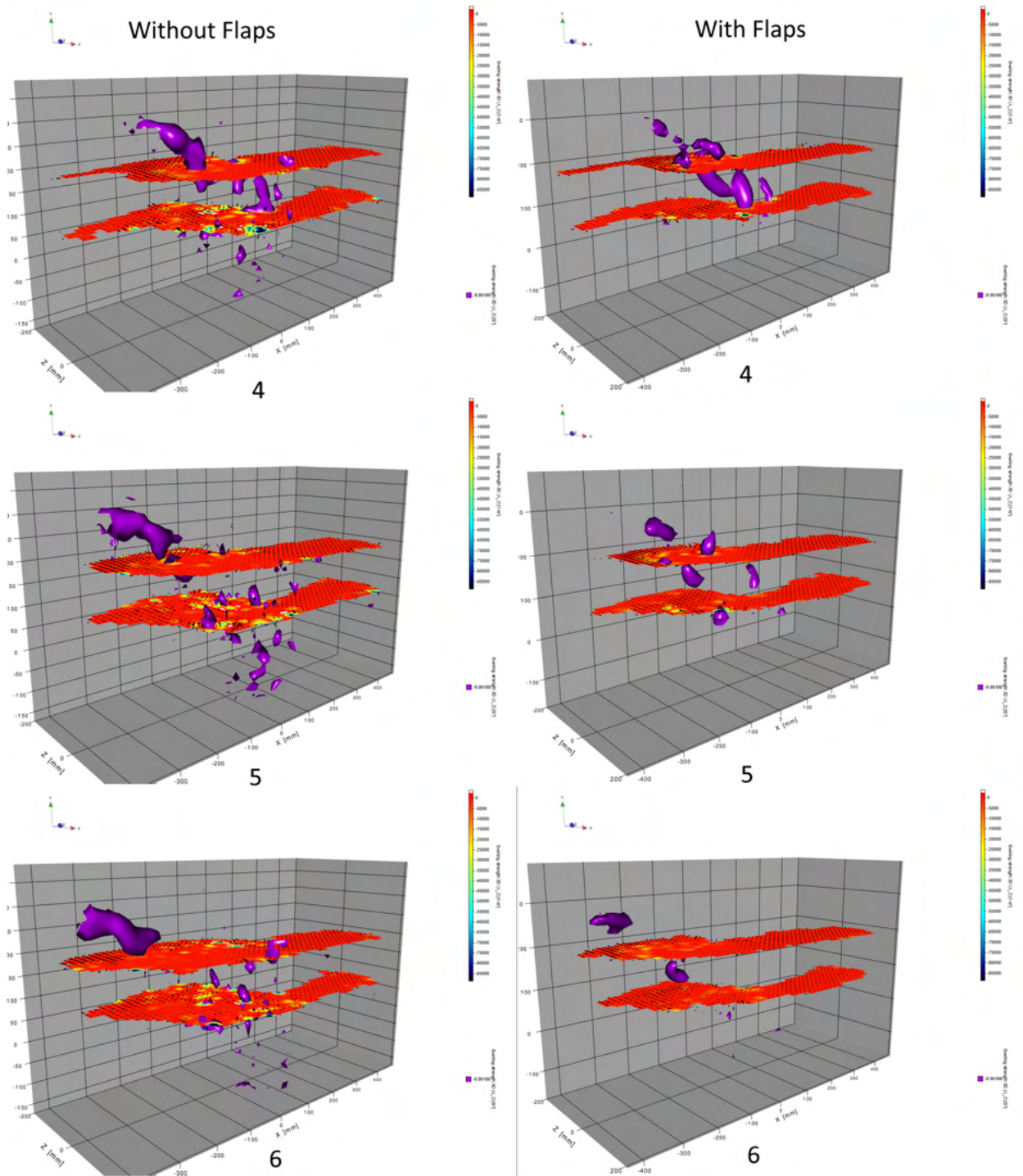


Figure 25: Snapshot 4 to 6 of the λ_2 criteria data in the voxel space of left without flap and right with flap.

5 Discussion

This section discusses the things that happened during the experiments that might be of influence on the results. It will be described what these things are and if and in what way they influenced the results. The division between the two experiments is also used in this section.

5.1 Static Testing Using a Load Cell on an Airfoil

One of the discoveries made during initial testing was the fact that the first airfoil, sized according to the paper by Izquierdo et al. [10], was too large for the wind tunnel. This was because at higher angles of attack the blockage ratio got as high as almost 30 %, which meant that the data was not accurate anymore. To solve this problem, a scaled down airfoil was produced of which the chord length was half of that of the first one. The maximum angle of attack was furthermore limited to 25° which reduced the maximum blockage ratio to 13.8 %. In order to then keep the same Reynolds number the wind speed had to be increased two fold to 26.3 m s^{-1} . Increasing the wind speed has a negative impact on the blockage ratio but compared to the half sized airfoil it is almost negligible.

As a result of this change, also all the dimensions of the paper flaps had to be shrunk by 50 %, in order to keep the conditions the same. This did have some consequences for the relative stiffness of the flaps, as the stiffness could not be scaled down by for example also cutting the thickness of the paper in half. All of these solutions had changed the experiment significantly which lead to the decision to not exactly recreate the experiment by Izquierdo et al. [10]. Instead it was used as a starting point to be in the right ballpark of flap influence on flight characteristics.

Inspired by the before mentioned paper, tape was used to attach the paper flaps to the airfoil. This showed to be an effective and easy solution to this problem. One drawback that occasionally occurred was the fact that because of all the fluttering and moving of the flaps the tape would peel back a little bit as can be seen in Figure 26. One time, the experiment was retried after the tape had peeled back a bit and the data was compared. This did indeed show that the suspicion of this having an effect on the results was true, however this effect was small. This can be mainly seen in the results of the flaps with different lengths as these were executed twice. Eventually based on these results the decision was made to keep the tape and keep an eye on how the tape was behaving and reattaching when necessary.

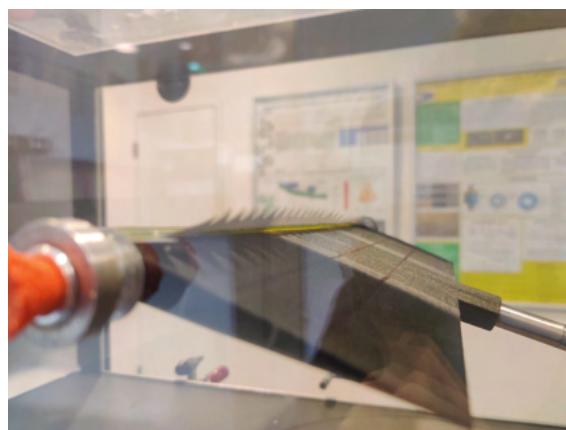


Figure 26: *Picture of the tape peeled back by a bit.*

As was mentioned in section 3.1 a 100 data polls were done for each angle measured. This was done due to the vibrations and fluttering behaviour of the flaps, which resulted in the values of the force sensors not being completely stable. This way the average force for each angle could be calculated and was used in the results.

Results 4.1.1 Different Flap Shapes:

A number of shapes were tested at two different lengths, at a length of 10 mm in Figure 13a a clear performance difference can be seen in the lift coefficient. The square flap (BICF 1) did significantly better than the small triangle flap (BICF 4). At the length of 32.5 mm almost no difference can be seen between the same shaped flaps. This is likely due to the fact that the angle of the triangular tip at the end of the flaps was not changed relative to the length of the flap. Meaning that for the

32.5 mm flaps the small triangle shape (BICF 4) was more similar to the square shape (BICF 1) than it was for the 10 mm flaps. The data for the large triangle shape (BICF 5) further agrees with this statement. In figure 13b it can be seen that for this shape there was almost no significant change in lift coefficient compared to no flaps (Reference case). Therefore it makes sense that the 10 mm small triangle flap (BICF 4) performs worse since it is closer to the large triangle shape (BICF 5).

The data for the 32.5 mm BICF 5 flap together with the observations seems to suggest the fluttering plays an important role in the lift improvements since for this flap there was almost no improvement gain. And as mentioned in the observations there was not significant fluttering for these flaps.

Results 4.1.2 Different Flap Lengths:

Because of the results for the different shapes tested, it was decided to use only the square shape (BICF 1) to measure different lengths. The data in Figure 14 first of all shows that all length flaps had a significant increase in the coefficient of lift compared to the reference case.

Furthermore, from these results good insight were obtained about the repeatability of the experiment. Due to a suspicion of the experiments leading to different results because of small perturbations in variables such as the tape letting go. It was decided to repeat all of the different lengths. From this graph it can be seen that there is indeed a small difference between the repeated experiments, however most of this data falls within the error boxes.

An interesting note is that the data seems to suggest there is an optimum length for the flap since the improvements first grow with the length of the flaps and later start degrading for the longest flaps tested.

Results 4.1.3 Different Flap Locations:

Interestingly the flap that had the biggest improvement so far on a quarter chord did not perform very well on the three quarters of the chord length. As can be seen in Figure 15 the flap managed to decrease the lift for angles smaller than the stall angle. This has so far not been observed with the other flaps.

Results 4.1.4 Different Reynolds Number:

In the experiments of the results in Figure 16a and 16b the difference between two Reynolds numbers was measured. This was done to see how and if this would influence the results. The flaps that were taken were used since they ranged from big improvements to small improvements and in between. It is interesting to see, that although the improvements and changes in the lift coefficient differ from each other, for both Reynolds numbers the same flaps had the same kind of improvements over the reference case.

The blue and red line in figure 16a show also some interesting behaviour between 10 and 15 degrees but no further research was done to find out why this was the case.

Results 4.1.5 Double Flaps:

The results for the double flaps is very promising as the small 10 mm square flap added to the 32.5 mm BICF 5 flap increased the lift coefficient over the whole range. There was not enough time to try out more combinations and go further along this path, but this path is recommended for further research.

5.2 Dynamic Testing Using the PTV Setup on the RoBird Wing

In table 2 it can be seen many different setups and measurements have been done. Since it proved rather hard to create reliable data or take reliable measurements the data set with the most promising data between the two scenarios (with and without flaps) was chosen. This meant that for

these data sets a lot of particles were tracked and only a small amount of ghost particles were present.

In the left row of Figures 24 and 25 (without flaps) the vortex or purple blob seems to be further in the process of becoming the tip vortex. This data has been analyzed in the program where it was possible to take a better look at the difference between these blobs in the same time frame for the different cases. In frame 3 of these Figures the difference is most notable, where at the left side (without the flaps) the vortex has gotten a lot further down the wing and is more broken up than the one on the right (with the flaps), which is still a more coherent structure.

This same observation continues during frame 4 and 5. however the vortex for the wing with the flaps in frame 5 seems to be splitting up and almost disappearing completely. In frame 2 the blob is bigger and thus already seems to start detaching from the airfoil.

A point of discussion is the fact that the error has not been Incorporated in the results shown in Figures 24 and 25. The particle tracks themselves of course have an uncertainty which gets translated to an uncertainty in the vector field. Furthermore when doing calculations on this vector field the errors propagate and should be taken into account.

There are some good indications that the data is of good quality, such as the small amount of ghost particles and in Figure 27 it can be seen how the lambda-2 criteria detects a, in this case, tip vortex. However the data needs to be analyzed further to be sure about the findings based on this data.

Even though there is a lot of information in the PTV data, it proved to be hard to extract

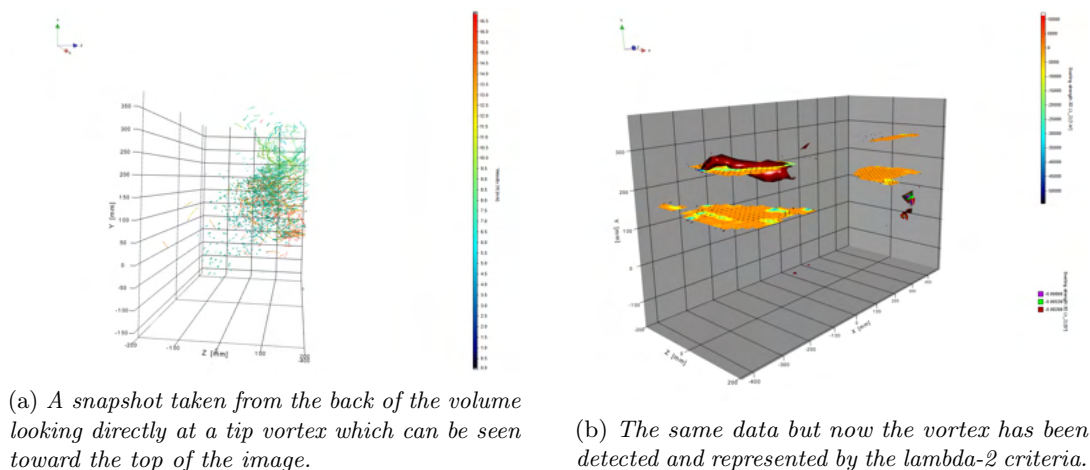


Figure 27

all of this information. Judging only by the LEV how the airflow around the wing is influenced exactly was limiting. The addition of a force torque sensor could have been very useful. Not only to see which feathers or flaps would perform better or worse, much like the first experiment in the small wind tunnel, but also verify what can be seen in the PTV data, such as the idea that an LEV that detaches later does indeed increase the lift for larger angles of attack.

An interesting observation that was made while analyzing the data is that this method visualised the LEV turning into the tip vortex rather nicely. The purple blob starts of in line with the wing and transitions throughout the frames into the tip vortex which is perpendicular to the wing.

A similar method to the first experiment was used to attach the tape to the wing. However since reapplying would not be possible due to all the soap, an extra measure was taken to improve the strength of this hinge. A layer of double tape was used under the attachment place of the flap to make it stronger.

Finally another problem that often arose was the bubbles not seeding properly. Meaning that when the HFSB was turned on it often needed to be turned off and on again once more to get bubbles forming out of all nozzles.

5.2.1 Planning

All the way in the beginning the plan was to have wind tunnel time in the month of April, however because things go as they do the planning ended up being 2 weeks in May. The more important thing about this is the fact that it was only 2 weeks. Earlier that month there was a problem with the laser and it was sent back to the Lavisision for a repair / replacement. Because of this at the moment of starting to build up the setup there was no laser yet and it was not certain if the experiments could even be done. Luckily it arrived only one day later than planned and this was not too much of a setback. A different setback in the planning was the fact that wind tunnel test frame was disassembled. Therefore part of the 2 weeks that I had planned for building the setup and measuring now needed to be dedicated to building this frame back up. This ended up taking the full first of the two weeks and only in the second week the actual measurement setup was started on. By Wednesday in the second week the setup was finally build and since on Friday the setup would already have to be taken down for to clear out the wind tunnel for the next week there was initially only 1 day of testing. Luckily the due to a change in planning the Monday could be used for taking down the setup such that 2 full days of testing were available.

5.2.2 Ghost Particles

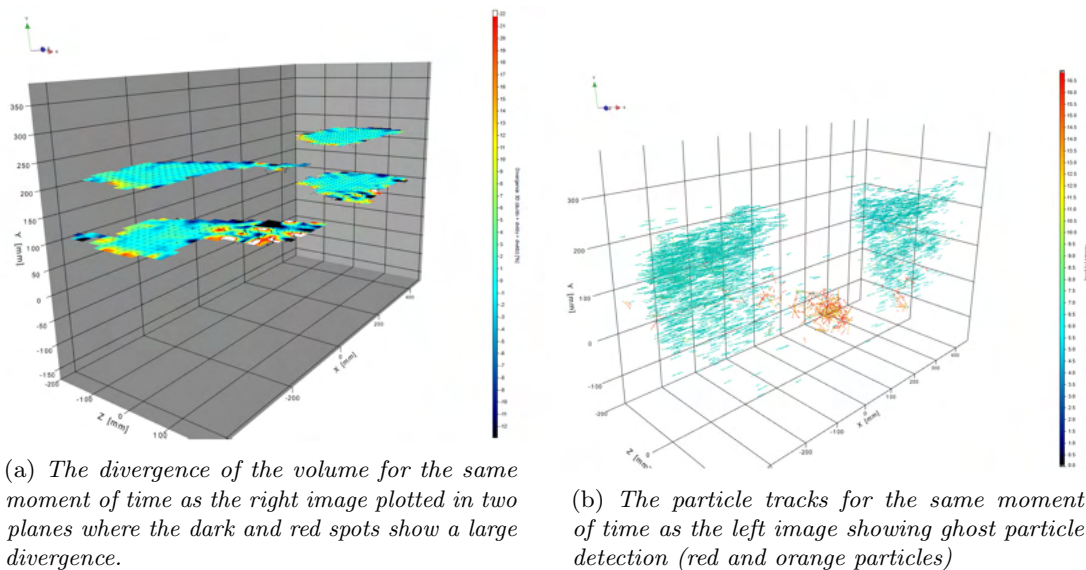


Figure 28

During PTV measurements it is important to make sure that the footage that is captured is of good quality, in focus and properly calibrated. If this is not the case the shake-the-box algorithm is going to have a hard time finding particle tracks. When the data itself is poor it can result in either less or almost no particle tracks (no usable data) or a few or many faulty particle tracks (messy data). These particle tracks which are wrongly detected are called ghost particles, as they technically do not exist but the algorithm thinks they do. This became very clear during the first few measurements as the data was not good enough for the algorithm to find a substantial amount

of particle tracks. The settings were then tweaked such that the threshold was set lower to be able to detect more particles which ended up in a lot of ghost particles.

A small example is given in Figure 28b where the ghost particles can be recognized by their red yellow colour. The colour indicates the velocity of the particle and for these particles the velocity is too high in the wrong direction for them to be able to actual particle tracks.

A reason for these particles being detected wrongly is because the wing obstructs the view of one or two cameras at certain angles of flapping. This means that for those moments the algorithm only has two or three cameras to resolve the location of these particles and is therefore not always able to do so properly. Finally, the way the data which was used for the results was tested on the divergence to see if the measurements were valid enough, this was done by calculating the divergence as explained in 2.4.2. In Figure 28 a good example can be seen of the divergence not being zero where there are ghost particles, and thus the flow would not be incompressible, making the data less useful.

5.3 Static Testing Using the PTV Setup on a 3D Printed Wing

Another experiment was set up and executed hastily between the two main experiments. This was done because there was suddenly an opportunity to be able to access the wind tunnel with the whole PTV setup already installed. Since normally this setup costs a lot of time to set up it was a valuable opportunity to do some measurement or at least get used to how the setup works.

The data gathered during the experiment turned out to not be very useful partially due to the speed with which everything had to be done. The opportunity was however still very useful as a lot was learned about how the setup worked and what to look out for when setting it up or work with it, this made the main experiment go a lot smoother. Furthermore during these experiments the helium ran out and because a new bottle was not immediately available the opportunity was over.

6 Conclusion

In this section a conclusion will be given to both research questions after they are repeated, these research questions fall in line with the two experiments done and thus each have their own subsection.

6.1 Static Testing Using a Load Cell on an Airfoil

RQ2: "Which of the selected imitated covert feather designs lead to (the largest) improvements in lift at high angles of attack in static flight"

Through the method used, a most effective flap shape was found. This was tested at different lengths after which the best performing one was selected. This flap was tested at different locations on the wing and in different scenarios by changing the Reynolds number. Therefore it can be concluded that the imitated covert feather design which lead to (the largest) improvements in lift at high angles of attack in static flight was the square shaped flap or BICF 1 at a length of 32.5 mm and a width of 10 mm at a location of $\frac{1}{4}$ chord length. This translates into a ratio of 0.332 x/c (x being the flap length). A lift enhancement of about 35 % at angles of attack higher than 18° was measured.

6.2 Dynamic Testing Using the PTV Setup on the RoBird Wing

RQ 1: "How does the lifting of covert feathers during high angle of attack manoeuvres influence the airflow over the wing?"

After the appropriate flap was selected, PTV measurements were done with this flap to gain insight on how the lifting covert feathers influence the airflow over the wing. Through the PTV data using the lambda-2 criteria for detecting vortices, the movement of the LEV was analyzed. Through these results it can be concluded that there is a small but significant difference between the moment of detachment of the LEV for the with and without the flaps. The LEV for the wing with flaps is about 20 frames or 100 ms behind on the LEV for the wing without the flaps.

Based on only these results no conclusion can be made on if this delay in detachment of the LEV could be advantageous for the flapping high angle of attack manoeuvres of a bird. More research is needed for more flaps, scenarios, and arrangements to be able to make a conclusion. Further recommendations are done in section 7.

7 Recommendations

For the first results it was not possible to do all the analysis that could have been done. This leads to the recommendation to further investigate and characterise the flaps and their behaviour for the static case. Using the Cauchy number as analysis tool to be able to relate the behaviour of the flap to the design parameters under various circumstances. This could for example fill the gap of research for the stiffness parameter of the flaps which could have a great influence but was not taken into account in this research.

The research is done on a flapping wing at a static angle of attack. In landing and perching manoeuvres the wing undergoes a (rapid) pitch up manoeuvre. This is another regime on which not a lot of research has been done but which could lead to interesting results since it is another step closer to the full manoeuvre of the bird. Furthermore it is possible to then combine this pitch up motion with a flapping wing.

The method used proved to be a good way to detect and produce a leading edge vortex. This could be used to test for more cases and flaps to broaden this research. Furthermore it could serve as a tool for other research surrounding the leading edge vortex.

One recommendation to improve the setup would be to add a force torque sensor such that data from this can be used in parallel to the PTV data. Having access to that data could give a lot more insight into the same experiment which would be a big improvement for a relatively small cost.

In this research a threshold was set for the vortex criteria, but it would be interested to look at the vortex strength, and analyze the data again based on this measure.

8 Appendix

8.1 Measurement plan for the static experiments in the small wind tunnel 3.1

1. Start the wind tunnel
2. Open the panel
3. Put the airfoil in place
4. Tighten the set screw
5. Close the panel
6. Lock the panel
7. Set the angle using the attitude knob to 0 degrees
8. Zero the force sensors
9. Take picture of setup
10. Make sure the winds speed is set to automatic and 0
11. Enable the VFD of the wind tunnel
12. Slowly build up the wind speed
13. For the first time keep an eye on the forces such that they do not exceed the maximum forces
14. Continue until the desired velocity is reached
15. Wait for the airspeed to stabilize
16. Take n amount of measurements with the auto clicker, at the fastest speed because of time, 30 ish milli seconds
17. Change the angle by one degree using the attitude control knob
18. Take another measurement and keep observing the airfoil
19. Repeat this process for all the desired angles taking measurements using the auto clicker
20. As soon as the last step is reached turn off the wind tunnel fan
21. Save the file under a file name with the experiment details in it
22. Unscrew the set screw
23. Take out the airfoil
24. Add the desired BICF to the airfoil by taping it on
25. Re seat the airfoil in the wind tunnel
26. Repeat the same steps over to do all the measurements necessary.
27. Repeat this for all the desired BICF's and or locations

References

- [1] Chelsea Gohd. ‘Meet Relativity Space: the little 3D printing rocket company that could’. In: *Space.com* (13th Jan. 2022). URL: <https://www.space.com/relativity-space-company-terran-1-launch> (visited on 03/07/2022).
- [2] Vishal Singh. ‘German drone startup Wingcopter secures €39.7M; plans to hire 80 new employees’. In: *Silicon Canals* (23rd June 2022). URL: <https://siliconcanals.com/crowdfunding/wingcopter-secures-39-7m/> (visited on 03/07/2022).
- [3] *The Drone Bird Company*. <https://www.thedronebird.com/>. Accessed: 2022-07-04.
- [4] Abdulghani Mohamed et al. ‘Fixed-Wing MAV Attitude Stability in Atmospheric Turbulence—Part 2: Investigating Biologically-Inspired Sensor’. In: *Progress in Aerospace Sciences* (July 2014). DOI: 10.1016/j.paerosci.2014.06.002.
- [5] *The Portwings Project*. <http://www.portwings.eu/>. Accessed: 2022-07-04.
- [6] Anna C Carruthers, Adrian LR Thomas and Graham K Taylor. ‘Automatic aeroelastic devices in the wings of a steppe eagle *Aquila nipalensis*’. In: *Journal of Experimental Biology* 210.23 (2007), pp. 4136–4149.
- [7] Chengfang Duan, Josiah Waite and Aimy Wissa. ‘Design optimization of a covert feather-inspired deployable structure for increased lift’. In: *2018 Applied Aerodynamics Conference*. 2018, p. 3174.
- [8] Chengfang Duan and Aimy Wissa. ‘Covert-inspired flaps for lift enhancement and stall mitigation’. In: *Bioinspiration & Biomimetics* 16.4 (2021), p. 046020.
- [9] Gotz Bramesfeld and Mark D Maughmer. ‘Experimental investigation of self-actuating, upper-surface, high-lift-enhancing effectors’. In: *Journal of aircraft* 39.1 (2002), pp. 120–124.
- [10] David OD Izquierdo and Flávio D Marques. ‘Experimental analysis of passive bio-inspired covert feathers for stall and post-stall performance enhancement’. In: *Meccanica* 56.11 (2021), pp. 2671–2689.
- [11] Aaron Altman and Guillaume Allemand. ‘Post-stall performance improvement through bio-inspired passive covert feathers’. In: *54th AIAA Aerospace Sciences Meeting*. 2016, p. 2042.
- [12] Christopher D Griffin et al. ‘Free flight observations and aerodynamic analysis for biologically-inspired optimization’. In: *55th AIAA Aerospace Sciences Meeting*. 2017, p. 0501.
- [13] Xia Wang and Julia A Clarke. ‘The evolution of avian wing shape and previously unrecognized trends in covert feathering’. In: *Proceedings of the Royal Society B: Biological Sciences* 282.1816 (2015), p. 20151935.
- [14] Tobin L Hieronymus. ‘Flight feather attachment in rock pigeons (*Columba livia*): covert feathers and smooth muscle coordinate a morphing wing’. In: *Journal of anatomy* 229.5 (2016), pp. 631–656.
- [15] Thomas Willem Bachmann. ‘Anatomical, morphometrical and biomechanical studies of barn owls’ and pigeons’ wings’. PhD thesis. Aachen, Techn. Hochsch., Diss., 2010, 2010.
- [16] Reinhold Necker. ‘Observations on the function of a slowly-adapting mechanoreceptor associated with filoplumes in the feathered skin of pigeons’. In: *Journal of Comparative Physiology A* 156.3 (1985), pp. 391–394.
- [17] Scott Hickman. ‘The trouble with tertials’. In: *The Auk* 125.2 (2008), pp. 493–493.
- [18] Irby J Lovette and John W Fitzpatrick. *Handbook of bird biology*. John Wiley & Sons, 2016.
- [19] Hugh Dingle. ‘The Sibley guide to birds’. In: *Science* 293.5537 (2001), pp. 2002–2002.
- [20] Christopher D Griffin et al. ‘Free flight observations and aerodynamic analysis for biologically-inspired optimization’. In: *55th AIAA Aerospace Sciences Meeting*. 2017, p. 0501.
- [21] Marco KleinHeerenbrink et al. ‘Optimization of avian perching manoeuvres’. In: *Nature* (2022), pp. 1–6.

- [22] Lawrence W Carr, Kenneth W McAlister and William J McCroskey. *Analysis of the development of dynamic stall based on oscillating airfoil experiments*. Tech. rep. 1977.
- [23] Amanullah Choudhry et al. ‘An insight into the dynamic stall lift characteristics’. In: *Experimental Thermal and Fluid Science* 58 (2014), pp. 188–208.
- [24] D Arivoli, Ishan Singh and P Suriyanarayanan. ‘Rudimentary emulation of covert feathers on low-AR wings for poststall lift enhancement’. In: *AIAA Journal* 58.2 (2020), pp. 501–516.
- [25] John Anderson. *Fundamentals of Aerodynamics (SI units)*. McGraw Hill, 2011.
- [26] Justin Winslow et al. ‘Basic understanding of airfoil characteristics at low Reynolds numbers (10 4–10 5)’. In: *Journal of Aircraft* 55.3 (2018), pp. 1050–1061.
- [27] Max F Platzler et al. ‘Flapping wing aerodynamics: progress and challenges’. In: *AIAA journal* 46.9 (2008), pp. 2136–2149.
- [28] Bernard S Massey and John Ward-Smith. *Mechanics of fluids*. Crc Press, 2018.
- [29] Qing Mei et al. ‘Structure light telecentric stereoscopic vision 3D measurement system based on Scheimpflug condition’. In: *Optics and Lasers in Engineering* 86 (2016), pp. 83–91.
- [30] B Wieneke. ‘Volume self-calibration for 3D particle image velocimetry’. In: *Experiments in fluids* 45.4 (2008), pp. 549–556.
- [31] Daniel Schanz, Sebastian Gesemann and Andreas Schröder. ‘Shake-The-Box: Lagrangian particle tracking at high particle image densities’. In: *Experiments in fluids* 57.5 (2016), pp. 1–27.
- [32] Ming Jiang, Raghu Machiraju and David Thompson. ‘Detection and visualization of’. In: *The visualization handbook* 295 (2005).
- [33] Jinhee Jeong and Fazle Hussain. ‘On the identification of a vortex’. In: *Journal of fluid mechanics* 285 (1995), pp. 69–94.
- [34] Jewel B Barlow, William H Rae and Alan Pope. *Low-speed wind tunnel testing*. John Wiley & Sons, 1999.
- [35] H Julian Allen and Walter G Vincenti. ‘WALL INTERFERENCE IN A TWO-DIMENSIONAL-FLOW WIND TUNNEL, WITH’. In: *Annual Report of the National Advisory Committee for Aeronautics* 268 (1949), p. 155.
- [36] EC Maskell. *A theory of the blockage effects on bluff bodies and stalled wings in a closed wind tunnel*. Tech. rep. Aeronautical Research Council London (United Kingdom), 1963.
- [37] Aerolab. *Educational Wind Tunnel (EWT) Aerolab*. <https://www.aerolab.com/aerolab-products/educational-wind-tunnel-ewt/>. Accessed: 2021-12-22. 2021.
- [38] Airfoil Tools. *SD7003-085-88 (sd7003-il)*. <http://airfoiltools.com/airfoil/details?airfoil=sd7003-il>. Accessed: 2022-08-15. 2022.
- [39] University of Twente. *AeroAcoustic Windtunnel*. <https://www.utwente.nl/en/et/tfe/research-groups/facilities/wind-tunnel/>. Accessed: 2022-06-13. 2022.
- [40] LaVision. *Helium-filled Soap Bubble Generator*. <https://www.lavision.de/en/download.php?id=2677>. Accessed: 10-08-2022. 2018.